NIRL/R/78

THE NATIONAL INSTITUTE
FOR RESEARCH IN NUCLEAR SCIENCE

PULSED HIGH FIELD MAGNETS

by

J. D. Milne

K. D. Srivastava

M. N. Wilson

Nimrod Beams Physics Group
RUTHERFORD HIGH ENERGY LABORATORY
CHILTON, DIDCOT, BERKSHIRE
1964

NIRL/R/78

NATIONAL INSTITUTE FOR RESEARCH IN NUCLEAR SCIENCE

PULSED HIGH FIELD MAGNETS

by

J. D. Milne

K. D. Srivastava

M. N. Wilson

ABSTRACT

The report describes an investigation into the feasibility of using pulsed high magnetic fields for experiments with Nimrod.

Nimrod Beams Physics Group,
Rutherford High Energy Laboratory,
Chilton, Didcot, Berkshire.

November, 1964.

CONTENTS

CONTENTS

LIST OF ILLUSTRATIONS

Figs.

1. INTRODUCTION

1.1 Application of High Magnetic Fields in High Energy Physics

For the purpose of this report 'high magnetic fields' are defined as fields which are above the region accessible to conventional iron yoke magnets. These conventional magnets are usually preferred in high energy physics experiments for their economy and accuracy of field in space and time, but there are some situations in which the use of higher fields is desirable. Two of these are briefly described below.

(a) Nuclear Emulsion Experiments

In a dense medium such as a nuclear emulsion, coulomb scattering effects are large, and may, over short distances, obscure attempts to measure the charge or momentum of a particle by its deflection in a magnetic field. Typical figures are: at 1GeV with a track length of 1 cm. in a field of 20 kilogauss, the magnetic deflection = 6 milliradians, and the coulomb scattering = 7.5 milliradians. Clearly, even the sign of the particle is in doubt here, and magnetic fields in the range of hundreds of kilogauss are called for. Pulsed high field techniques, in particular, have been used with nuclear emulsions in many accelerator laboratories, notably at C.E.R.N.[1]

(b) Experiments Involving Unstable Particles

Magnetic measurements on particles which decay in a few centimetres need high magnetic fields to produce a significant deflection over the short distance. Of interest here are the measurements of the magnetic moments of Σ^+ and Λ^0 particles using emulsions,[1] spark chambers[2] and a cloud chamber.[3] Smaller fields of 60 kilogauss have been used to momentum analyse a low energy kaon beam.[4]

1.2 Generation of High Magnetic Fields

The choice of a suitable method of generating high magnetic fields is governed by considerations of field magnitude, volume, geometry and duty cycle. Continuous fields are produced either by conventional methods using large rotating machines or by superconducting coils. Conventional magnets require several megawatts of d.c. power, and the maximum d.c. field produced by this

method is about 250 kilogauss.[5] The maximum field produced so far by a superconducting coil of reasonable volume is 100 kilogauss; this figure is unlikely to be very much exceeded in the near future.

For pulsed magnets the energy is usually stored in some suitable form, e.g. fly-wheels, batteries, inductors and capacitors, and is delivered to the magnet coil in pulses through appropriate switches. The choice of the most economical form of energy storage depends upon the required magnitude and duration of the field pulse as well as the duty-cycle.[6] Rotating machines with fly-wheels are economical when the pulse duration is several hundred millisecs and the stored energy several megajoules. On the other hand, inductors are suitable if the stored energy does not exceed a few hundred kilojoules and for pulse durations of well under 100 millisecs. Switching problems for inductors are particularly troublesome. Batteries have been used for field pulses of several hundred millisecs. duration, but their initial cost is usually high and they are unsuitable when faster repetition rates, (a few pulses per minute), are required.

Capacitor banks have so far proved very versatile for pulse durations ranging from a few microsecs. to somewhat over 100 millisecs. and for stored energies up to several megajoules. They are almost the only suitable form of energy storage for fast pulses ($\approx 10\mu$secs), albeit their cost increases with decreasing pulse durations.

1.3 Scope of Investigation

The present investigation was undertaken with a view to developing pulsed magnets for over 200 kilogauss, which could be used for nuclear emulsion experiments with the 7GeV proton synchrotron, NIMROD. The fast extraction system on Nimrod is expected to produce a proton burst of 50 μsec. duration. A magnetic field pulse of about 500 μ secs half period, suitably synchronised to be symmetrical about the proton pulse, would ensure that the field did not vary by more than 2 percent over the duration of the proton pulse. At C.E.R.N. a system of pulsed magnets had been developed for nuclear emulsion experiments on the C.E.R.N. proton synchrotron.[7] [8] These magnets generate a field of over 200 kilogauss with a useful volume of approximately 500 cc. The

energy is stored in a 300 kilojoule capacitor bank at 2.8 kilovolts. The pulse duration of these magnets is approximately 5 millisecs. half-period, and the life of each magnet is about 3000 pulses. It was decided to improve the life of these magnets, and extend this work to magnets for shorter pulse duration - bearing in mind that it may be possible to use these magnets for experiments with the C.E.R.N. proton synchrotron; the fast extraction system on this machine is expected to produce proton pulses of 1 - 3μsec. duration.

Reducing the pulse duration affects the capacitor bank design. For efficient transfer of the capacitor energy to magnetic energy it is necessary that the resonant frequency of the capacitor bank should be considerably higher than the discharge frequency of the magnet pulse. Since for a given container size, there is a minimum connection inductance inherrent in a capacitor unit, improvement of the resonant frequency is usually achieved by reducing the capacitance per container. For reasons of economy it becomes necessary to operate the capacitor units at a higher voltage so that the energy stored per unit remains unchanged. The British capacitor manufacturers indicated, on our enquiry, that an operating voltage of 10 - 14 kilovolts would be necessary if a resonant frequency of 100 - 200 kc/s was required.

Pulsed magnets are usually of two types: helical coils (Bitter type), or transformer coils (e.g. flux-concentrators). Bitter coils are more efficient, but their life is limited by the failure of the inter-turn insulation; this is further aggravated by operating these coils at a higher voltage. Transformer coils on the other hand, are mechanically robust but suffer from poor inductive efficiency. The present investigation has therefore been concentrated on two aspects of pulsed high field magnets:

(a) Improvement of insulation and life of Bitter type coils operating at 10 kilovolts.

(b) Improvement of efficiency of transformer coils.

Most of the work reported here was carried out with a 480 μF, 20 kilovolts capacitor bank which was available in the Laboratory. The resonant frequency and the stored energy were both smaller than those needed for pulse

magnets for emulsion experiments. However, these limitations did not affect the scope of the investigation.

The capacitor bank with its associated charging and switching circuits is described in Appendix 1. Various measuring techniques for voltage, current and magnetic field are also discussed in Appendix 1.

2. EXPERIMENTS WITH BITTER COILS

2.1 General

The requirement that a field pulse of about a hundred microseconds length must be produced using a capacitor bank of reasonable size means that the coil should have a self inductance of the order 10μ Henries i.e. a few dozen turns in a simple solenoid. The choice therefore lies between coils of the tape-wound and Bitter helix types. It has been the experience of other workers that, whereas the tape-wound coil is easier to manufacture than the Bitter helix, it is much worse in its support of mechanical stress. [17] Experimental applications in high energy physics usually require reliable operation over several thousand shots and so we have concentrated our efforts on the Bitter type of coil.

The experimental coils were not designed to meet any specific demand for a high field but rather to develop a manufacturing technique and to assess the peak fields and coil lifetimes which can be attained. No attempt was made, therefore, to produce a particular field shape (e.g. a region of uniform field using a Helmholtz pair), all the experimental coils were simple solenoids. It is the insulation between turns which mainly determines the peak field and lifetime of a Bitter coil and the largest part of our work has been directed towards finding the most suitable insulator. The most common cause of failure is mechanical crushing but, in addition, because energy storage is most economical at high voltage, the insulator must have a high dielectric strength. Good thermal shock properties are also needed because, during the field pulse, the temperature at the inner surface of the coil may rise by as much as 200°C.

Heat will diffuse into the main body of the helix with a characteristic time of about a second, raising its temperature by about 15°C. Some provision must therefore be made for cooling the coil if operation at rapid duty cycles is intended.

2.2 Magnetic Stresses

Calculations of the mechanical stress distribution in a cylindrical solenoid are given in Appendix 2 and the results applied to the third experimental coil. The forces operating may be divided into two types; bursting forces in the radial plane which principally affect the conductor, causing tensile failure at its inner edge, and axial contraction forces, acting mainly on the ends of the coil which cause the insulator to fail in compression. The distribution of these stresses may be modified to some extent by the application of external forces to precompress the coil. A force applied in the radial direction reduces the hoop stress at the inner edge (Figure A2.1) but generally puts extra load on the insulation. An axial precompressing force also increases the compressive load on the insulator but is usually necessary to prevent its failure in tension as the coil rebounds from its own axial forces. It is further shown in the appendix that, for a coil of given shape, the stresses brought about by both types of force increase as the square of the field but are independent of the size of the coil. We therefore expect that the materials and methods of construction which have proved most successful in our small scale experiments will prove equally successful on a larger scale and that the peak fields and lifetimes will be similar.

2.3 Experimental Tests

In Table I are listed the coils which have been manufactured and tested at high fields. The first three coils were of similar construction and appearance, consisting of a flat helical spiral machined from the solid metal with plastic insulation between the turns. No radial precompression was applied but the coils were constrained axially by massive end plates joined by high tensile bolts. The precompression applied was made equal to the total axial contraction force; at 200 k gauss the calculations of Appendix 2(b) show that for coil III this force is 1.6×10^4 k. gm. i.e. 16 tons. The joining bolts should be capable of supporting at least twice this load and the end plates should not deform

appreciably under it. Deformation was found to occur with the first set of plates which were slitted radially to reduce eddy current effects. These were replaced by solid plates which were separated from the ends of the coil by a sheet of "Tufnol" to allow space for the flux lines and thus keep the eddy currents small. In both cases the energy loss caused by these eddy currents had been calculated to be small and was not detected experimentally.

Coils I and II were made from Dural alloy because the Beryllium Copper was not readily available. Dural is inferior in both strength and conductivity but it was decided to go ahead with these coils in order to develop the machining and potting techniques and to obtain some preliminary results on insulation behaviour. In actual fact, the insulation failed first in both cases so that the ultimate strength of the conductor was of no consequence. Coil I failed after six shots at 170 k gauss and Coil II after 2000 shots at about the same field, indicating that reinforcement of the epoxy does substantially improve performance. These fields are much lower than the rough estimates made in Appendix 2(b), probably fatigue effects are important here. A suggestion has been made by Hoffmann[9] that a very tough insulating layer can be made by hard anodizing the Dural conductor; coils of this type have successfully been used with the 3kV. bank at C.E.R.N. Coil IIa, which is not included in the table, used the same helix as Coil II, this was hard anodized to the maximum possible depth of about 1 thou. and the closed helix was then vacuum potted to fill any pin holes. The insulation was found to be electrically unsatisfactory at the higher voltage however and the coil was destroyed by arcing at a low field.

In Coil III we set out to provide the maximum reinforcement for the epoxy insulator and the following technique was adopted.[10] The Berylco helix, after machining, was mounted on a mandrel which maintained the correct spacing between each turn (Figure 1) and a continuous filament of glass fibre was wound under tension into the gap between turns. The coil was then fitted into a glass fibre tube for additional support and vacuum potted in epoxy resin. Finally, the central mandrel was bored out, current contacts milled on the end faces and the coil mounted between the two end plates (Figure 2). The performance of this coil has been most satisfactory, the lifetime at 200 k gauss appears to be almost unlimited, no damage was observed after over four thousand shots at

210 k gauss. A further thousand shots at 260 k gauss produced no apparent damage to the insulation but increased the inner diameter slightly, indicating that the elastic limit had been exceeded, possibly with work hardening. This is in good agreement with the calculations of Appendix 2(a) and the published properties of Berylco 50. A single shot at 275 k gauss was then sufficient to destroy the coil, probably due to yielding of the conductor at its inner surface followed by arcing between turns. It may be possible to improve the performance of this type of coil still further by applying some radial precompression.

Coil IV was of a completely different design to the first three and was an attempt to utilise in the insulation the extremely high compressive strengths, and excellent thermal and electrical properties of sintered metal oxide refactories. The worst feature of these materials is their brittleness and weakness in tension, the coil design sought to avoid any tensile stress in the insulator by the use of both radial and axial precompression. Twelve slitted annular Berylco discs were stacked with ceramic segments between them and were brazed together to form a continuous helix. The complete assembly was then mounted on a mandrel and compressed axially (Figure 3); care had been taken to machine both sets of discs accurately flat so that the ceramic would not be damaged by this. After potting in epoxy to fill any small gaps, the outer diameter was ground to fit tightly into a thick walled ceramic tube and a steel hoop was shrunk onto the tube to compress the coil radially. Finally, the coil was mounted between end plates and the mandrel removed (Figure 4). A few dozen pulses at 200 k gauss produced no damage and the coil was taken in stages up to 270 k gauss. At this point arcing occurred at one of the end current leads, damaging the coil beyond repair, no sign of damage by mechanical stress could be seen however. It is felt that this method of construction shows some promise for the reliable production of fields in the 300 k gauss range.

3. TRANSFORMER COUPLED COILS

3.1 General

As a pulsed magnet, the single-turn coil is usually to be preferred to the multiturn type because it is mechanically much more robust and also because it produces a better field shape. At high frequencies, when the skin depth is small, the inner wall of the coil encloses a region of constant flux and fields of a given configuration may be produced by shaping the wall to fit the appropriate boundary conditions, i.e. that it should coincide with one of the required flux lines. In particular a region of uniform field may be produced in this way more easily than by using a multiturn coil where the flux penetrates the insulation between turns.[14]

The principal disadvantage of the single-turn coil is its low self inductance. This makes long pulses difficult to achieve, means that stray inductances in the discharge circuit must be kept very small and also raises problems of heavy current switching. The transformer coil offers a way of combining a multiturn coil in the primary winding with a single-turn coil as the secondary. The general theory of a transformer coil given in Appendix 3(a) shows that the effective inductance of the coil, as seen from the primary, is approximately $n^2 L_3$, where n is the number of primary turns and L_3 is the self inductance of the single-turn. Any single-turn coil may therefore be matched to a capacitor bank to give a certain pulse length simply by adjusting the number of primary turns. Several workers have successfully used transformer coils in this way, particularly in the form of the flux concentrator[15] [16] [17] [18] and all report that the principal drawback of the arrangement is its low energy transfer efficiency, typically about 15%. A larger capacitor bank is therefore needed to produce a given volume of magnetic field energy and, as the capacitor bank and its associated charging gear are by far the most expensive items of equipment, this low efficiency is a serious objection. We have developed an approximate theory of transformer systems, with special attention to their efficiency and the related problem of force containment, so that the optimum system for any particular experimental application may be designed and its usefulness compared with that of a multiturn coil. The theory has been checked at each stage by small scale experiments.

3.2 Energy

Appendix 3(a) presents a simple consideration of two coupled circuits using steady state A.C. theory, i.e. ignoring the resistive decrement which is usually small in practice. The theory is used to predict approximately the behaviour of the transformer coil as a circuit element and then to calculate its efficiency. Two sources of energy loss are present in the circuit, resistive dissipation of energy before the magnetic field reaches its maximum value and stray inductive energy, stored as magnetic field in parts of the circuit away from the high field region. The two are largely independent and are treated separately. Resistive losses, which are usually smaller than inductive losses depend simply on the primary and secondary resistances and the frequency of the discharge. These resistances are normally made as small as possible by providing a large area of winding and choosing suitable conducting materials. We follow Platner[18] in our treatment of inductive loss and define an inductive transfer efficiency as the ratio of the magnetic energy stored in the high field region to the total energy stored in the system. The efficiency is then obtained as a function of three dimensionless parameters, k, the coupling between primary and secondary, m, the coupling between secondary and single-turn (i.e. the load) and ℓ, the ratio of secondary to single-turn inductance. For particular values of k and m, the dependence of ϵ on ℓ is typically as shown in Figure A3·1 The maximum value of ϵ with respect to ℓ may then be plotted as a function of k and m as in Figure A3·2 In practice we usually have $m < 0.5$ so that the $m=0$ line approximately describes all cases of interest, obviously good coupling is essential for high efficiencies.

3.3 The Pulse Transformer

In Appendix 3(b) expressions for the coupling between primary and secondary current sheets are derived and it is shown that the coupling is increased by either decreasing the separation of the sheets or by increasing their area of contact (which incidentally also reduces the forces between them). These requirements suggest a method of construction similar to that of a capacitor and the first pulse transformer was accordingly made of copper foil interleaved with sheets of 'Melinex' insulating film. The primary turns were connected in series whereas the secondary turns were connected in parallel and brought together to form a low inductance lead out as in Figure 5. Measurements

of primary inductance and resistance with the secondary open and short circuited were substituted into the relations of Appendix 3(a) to obtain the resistance and inductance of the primary and secondary and the coupling constant between them. The effect of skin depth was investigated by making measurements at various frequencies. The measuring apparatus consisted of a Wayne Kerr type B221 Transformer ratio arm bridge driven by an audio oscillator and using a Wayne Kerr type A321 wave analyser as the tuned detector. The transformer was found to have good coupling ($k \simeq 0.995$) and the losses in the secondary leads were low, in addition, the forces acting everywhere were expected to be small because the currents were distributed over a large area. The worst problem encountered with this transformer was the technical one of taking current from the secondary leads to the single-turn coil without causing excessive leakage inductance or subjecting the layer structure to strong forces. Attempts to solve this problem or to design an alternative arrangement were not very successful and the idea of a pulse transformer with a separate single-turn coil was eventually discarded in favour of the simpler construction of the flux concentrator.

3.4 The Flux Concentrator

The secondary of the flux concentrator takes the form of a solid conducting slug with a radial slot joining the outer surface to the central hole. A changing current in the primary induces a circulating current in the secondary which is constrained by the skin effect to flow along the slot and round the central high field region (Figure 6). The coupling between the primary and secondary should be as great as possible and it is usual to increase their area of contact by embedding the primary in a helical groove cut into the secondary.[16] Many measurements of coupling were made by a comparison of the inductance and resistance of the primary when wound on an insulating former (secondary open circuit) with the inductance and resistance of the primary when wound on a slug with no slot (secondary short circuit). The results of these measurements are presented in Appendix 3(b).

Once it has been decided what value of 'k' can be obtained from a particular configuration of primary and secondary, the slug must be designed to have the required shape of high field region, to present to the external circuit the appropriate inductance for a given pulse length and to have the parameters ℓ

and m needed for optimum efficiency. The simplest shape of slug is the hollow cylinder of Figure 5. This is not strictly speaking a flux concentrator because the central field is about the same as the field in the slot and is approximately the field which would be produced by the primary current alone. The forces acting on the primary are greatly reduced by the helical groove type of winding, but where the primary crosses the slot it is still subject to large forces. There is also a large repulsive force between the two faces of the slot which sets up a bending moment on the body of the slug tending to open it out. To obtain higher fields in the centre it is clearly necessary that the slug should concentrate the current as it flows down the slot (Figure 6) thus producing a higher surface current density and hence a higher field in the central region than at the outer edge of the slot. Unfortunately this current concentration inevitably leads to an increase in the energy required to produce a given field energy in the centre and thus a decrease in the efficiency. If we consider a flux $\emptyset$ through the centre and assign to the inner surface as a whole a self inductance L, then for a total circulating current I we have:-

$$\emptyset = L\ I$$

$$\text{Energy} = \tfrac{1}{2} L I^2 = \frac{\emptyset^2}{2L}$$

The extra current paths on the end faces brought about by tapering (Figure 6) reduce the inductance of the inner contour and hence increase the energy required for a given $\emptyset$ and decrease the efficiency. The design problem has now become one of obtaining the current concentration required by force considerations without decreasing the self inductance of the inner surface too much. The analysis of Appendix 3(a) still holds good but the parameters ℓ and m must now apply to the whole inner contour and the efficiency derived will be the efficiency of energy transfer to this inner region. The useful high field energy will be some fraction of this.

An analogue which may prove useful in this design work has been described by Furth.[14] The flux in a cylindrically symmetric system may be represented by the potential in medium whose resistivity varies as $\frac{1}{r}$ i.e. by a resistance network or an electrolytic tank whose depth varies as $\frac{1}{r}$. If the r=o line is made to be one electrode and a two dimensional model of the inner

contour the other, then the potential difference between them represents the self inductance and the total current flowing represents the circulating current. Experimental measurements on actual flux concentrators show a very small azimuthal variation of the field due to the slot in most cases, thereby justifying the assumption of axial symmetry made above.

We have not carried out any analogue studies but a series of experiments has been undertaken in which the inner contour of a concentrator was progressively machined out and the fields and currents measured each time (column 3, Table II). It was found that the efficiency increased very slightly as more of the inside was removed, the efficiency of the final step shape being about 4% greater than that of the initial straight taper. Measurements with a small search coil in the slot however revealed that the current concentration with the step shaped inner was not uniform and that regions of high field existed in the slot near the primary. It was therefore decided that the straight taper shape should be adopted in the interests of prolonging the life of the primary.

In Appendix 3(c) we develop an approximate theory of the distribution of currents on the end faces of a tapered slug and use it to work out the current concentration, the total inductance of the inner surface and hence the reduction in efficiency. The value of concentration so obtained may be used together with an experimentally obtained value for the strength of the primary winding to predict the central field at which the primary will fail. The bending moment on the slug body may also be calculated and stress calculations (Appendix 3(d)) then give the field at which the slug body will yield.

3.5 Experimental Tests

In Table II we list the concentrators which have been pulsed at high fields by the condenser bank together with some of their theoretically predicted and experimentally measured properties. The list does not include many other coils which were either pulsed at low energy or used with the universal bridge to check the relations derived in Appendix 3. The first two concentrators were ad hoc designs in which the volume of high field was made to be about the same as that of the Bitter coils and the 'ℓ' parameter was adjusted for optimum efficiency. They were representative of the two principal types which had been made previously. It was noted with some surprise that both concentrators gave

exactly the same efficiency, in spite of the fact that great trouble had been taken to improve the coupling of the second type by using a solid primary which almost completely filled the helical groove, whereas the first type was series wound with Unipren power cable and had relatively poor coupling. Clearly this was due to the higher efficiency of the inner surface of the first. Concentrator 3 was pulsed at low energy with the inner contour machined successively to the five shapes shown, as mentioned previously. The concentrator, with a step shaped inner surface, was then pulsed at high fields and, as with No. 2, the cause of failure was found to be the primary insulation near the step. An additional concentrator No. 3a was also made, it was similar in size and shape to No. 3 but the central hole was offset towards the slot with a view to reducing the inductive energy loss in the slot. No gain in efficiency was observed but there was a marked increase in the azimuthal variation of field in the hole, failure was again due to the primary winding. Investigations of the end face currents were carried out at low energy with concentrator 4 and also at steeper angles using a longer slug; No. 4 was then pulsed at high energy. The shape of this slug was not very good from the current concentration or efficiency points of view and once again the primary windings failed at high field.

The final concentrator, No. 5, was the only one to be fully designed on the basis of the theoretical ideas already described. A peak field of 300 k gauss was required which indicated a current concentration about 3, if the primary was not to fail. The slug shown in Table II was chosen because it provided this concentration with the smallest reduction in efficiency. The stress calculations of Appendix 3(d), which assumed a steady load, indicated that the slug would open out at 145 k gauss. Although it was found experimentally that this figure could be exceeded by the actual impulsive loads, it was felt that for reliable operation over many shots, the slug should be able to support the steady load. Radial reinforcement was therefore provided by means of an outer Dural Tube (Figure 8). The tube was made to be electrically in contact with the slug body, probably somewhat improving the primary to secondary coupling. A slot was cut in the tube to coincide with slot in the slug and insulated bolts across this slug served to tighten the tube onto the slug. In its initial form with a 2 cm. diameter central hole, the concentrator produced a peak field of 305 k gauss. Failure occurred when the outer reinforcing tube fractured but the slug and primary were undamaged. The tube was repaired and the central hole enlarged to give a volume

of field comparable with that provided by the Bitter coils. A field of 210 k gauss was then obtained using the full bank energy of 42 kilojoules. After several shots, signs of incipient failure were again seen on the outer tube and pulsing was discontinued. Once again the primary winding and slug body were quite undamaged.

4. CONCLUSION

Techniques have been developed for designing a Bitter coil to reliably produce fields of 250 k gauss in a volume of 50 cm^3, operating at 10 k.V. These techniques are expected to be suitable for producing similar fields over a larger volume.

Experiments with transformer coils have demonstrated the reasons for their low energy transfer efficiency. The relationship between efficiency and magnetic stresses has been established and design criteria have been formulated. It has been possible to achieve efficiencies (28%) which are significantly higher that those reported previously and fields of over 300 k gauss have been obtained. Although this efficiency is still much lower than that of the Bitter coils (80%), the particular advantages of the single turn may outweigh this in certain applications.

5. ACKNOWLEDGEMENTS

Thanks are due to R. Sheldon of Chemistry Section for insulating the Bitter coils and to the Central Engineering Workshops for fabricating the Bitter coils and flux-concentrators.

Much of the experimental work on surface currents in flux-concentrators was done by K. B. Burchell, vacation student from Borough Polytechnic, London.

REFERENCES

1. 1962 Easter School for Physicists N. Doble W.O. Lock C.E.R.N. 63-3

2. R.L. Cool et al 1962 International Conference on High Energy Physics at C.E.R.N. p.345

3. W. Kernan et al 1962 International Conference on High Energy Physics at C.E.R.N. p.347

4. V.Z. Peterson "High Magnetic Fields" M.I.T., Wiley 1962, p.726

5. F. Bitter Review of Scientific Instruments Vol.33 No.3 p.342

6. R. Carruthers "High Magnetic Fields" M.I.T., Wiley 1962, p.307

7. The Design and Construction of a 200 kilogauss Pulsed Magnet M. Morpurgo et al C.E.R.N. 60-27

8. A 200 kilogauss Pulsed Magnet for Emulsion Experiments E. Braunersreuther et al C.E.R.N. 62-7

9. L. Hoffman, Private communication

10. J.D. Milne et al Review of Scientific Instruments Vol.35 No.9 p.1229

11. "Applied Elasticity" J. Prescott Dover Publications 1961

12. J.D. Cockroft Phil. Trans. Series A Vol.227 p.317

13. "Inductance Calculations" F.W. Grover Dover Publications 1962

14. H.P. Furth "High Magnetic Fields" M.I.T., Wiley 1962, p.235

15. Transformer Coils for High Magnetic Fields L. Hoffman et al C.E.R.N. 63-36

16. B. Howland et al "High Magnetic Fields" M.I.T., Wiley 1962, p.249

17. Y.B. Kim, E.D. Platner Review of Scientific Instruments Vol.30 No.7 p.524

18. E.D. Platner Thesis University of Washington

19. A Low Inductance Shunt for Measuring Heavy Current Pulses J.D. Milne et al Nuclear Instr. & Meth., October 1964

20. "The Strength of Materials" Part 1, Ch.12 S. Timoshenko Van Nostrand 1955

TABLE I BITTER COILS

COIL NUMBER	I	II	III	IV
Conductor	Dural N.E. 6 machined from solid	Dural N.E. 6 machined from solid	Berylco 50 machined from solid	Berylco 50 twelve sections brazed together
Insulator	Epoxy resin with silica flour filler	Epoxy resin with glass fibre cloth	Epoxy resin with continuous glass filament	Segments of "Deranox" sintered alumina
Number of turns	22	25	27	12
Inner diameter	3.8 cm	4.0 cm	3.6 cm	1.9 cm
Outer diameter	10 cm	10 cm	10 cm	3.2 cm
Axial length	4.0 cm	5.0 cm	5.2 cm	2.5 cm
Conductor thickness	1.0 mm	1.5 mm	1.2 mm	1.3 mm
Insulator thickness	0.8 mm	0.5 mm	0.7 mm	0.8 mm
Self inductance) at 1592 c.p.s.	11.5 μH	17.8 μH	13.9 μH	1.5 μH
resistance)	40 mΩ	29 mΩ	27 mΩ	6 mΩ
Performance	Insulation failed after 6 shots at 170 kilogauss	Insulation failed after 2000 shots at 170 kilogauss	4200 shots at 210 kilogauss 1000 shots at 260 kilogauss conductor yielded at 275 kilogauss	30 shots at 200 kilogauss destroyed by arcing at contacts at 270 kilogauss

TABLE II FLUX CONCENTRATORS

CONCENTRATOR NUMBER	1	2	3	4	5	
SLUG GEOMETRY	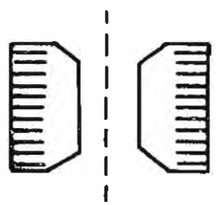	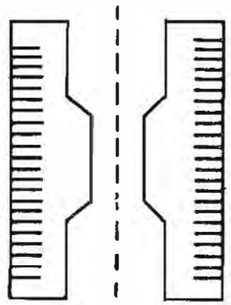	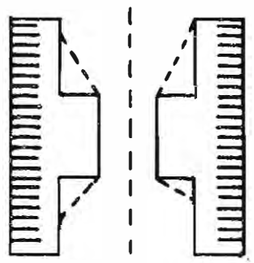	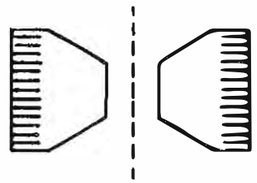	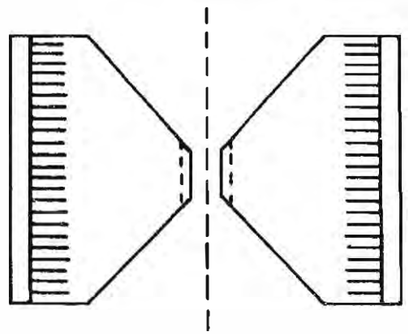	
PRIMARY WINDING	7 turns x 4 layers in series of Unipren 50 power cable	Dural Helix Epoxy insulated by fluidized bed coating	23 turns x 4 layers in parallel of Unipren 12 cable	12 turns x 5 layers in parallel of Unipren 24 cable	13 turns x 4 layers in parallel of Unipren 50 cable	
SLUG MATERIAL	Brass	Dural	Dural	Brass	Dural	
DIAMETER OF HIGH FIELD REGION	4 cm.	4 cm.	4 cm.	3.5 cm.	2.0 cm.	3.5 cm.
AXIAL LENGTH OF HIGH FIELD REGION	5.7 cm.	6.4 cm.	5 cm.	2.5 cm.	3.2 cm.	4.5 cm.
PRIMARY/SECONDARY COUPLING 'k'	0.96	0.990	0.987	0.985	0.983	0.983
ϵ_L CALCULATED (APPENDIX 3a)	0.56	0.73	0.70	0.68	0.63	0.68
ϵ'_L CALCULATED (APPENDIX 3c)	Not Calculable	Not Calculable	Not Calculable	0.31	0.26	0.29
Rp MEASURED	78 MΩ	31 MΩ	56 MΩ	19 MΩ	14 MΩ	15 MΩ
Lp MEASURED	21.8 μ H	6.8 μ H	12.4 μ H	3.7 μ H	3.4 μ H	4.2 μ H
TIME TO CURRENT MAXIMUM	140 μ sec	80 μ sec	100 μ sec	70 μ sec	60 μ sec	65 μ sec
ϵ_L MEASURED	0.40	0.40	0.34	0.38	0.29	0.28
ϵ TOTAL (INCLUDING RESISTIVE LOSSES)	0.27	0.29	0.24	0.28	0.23	0.23
ULTIMATE FIELD	93 Kilogauss	95 Kilogauss	100 Kilogauss	145 Kilogauss	305 Kilogauss	210 Kilogauss
CAUSE OF FAILURE	Mechanical Deformation of Slug	Insulation failure on Primary Winding	Primary Winding broken near the Slot	Slug Deformed and Primary Winding Broken	Reinforcing Dural Tube Broken	Reinforcing Dural Tube Broken

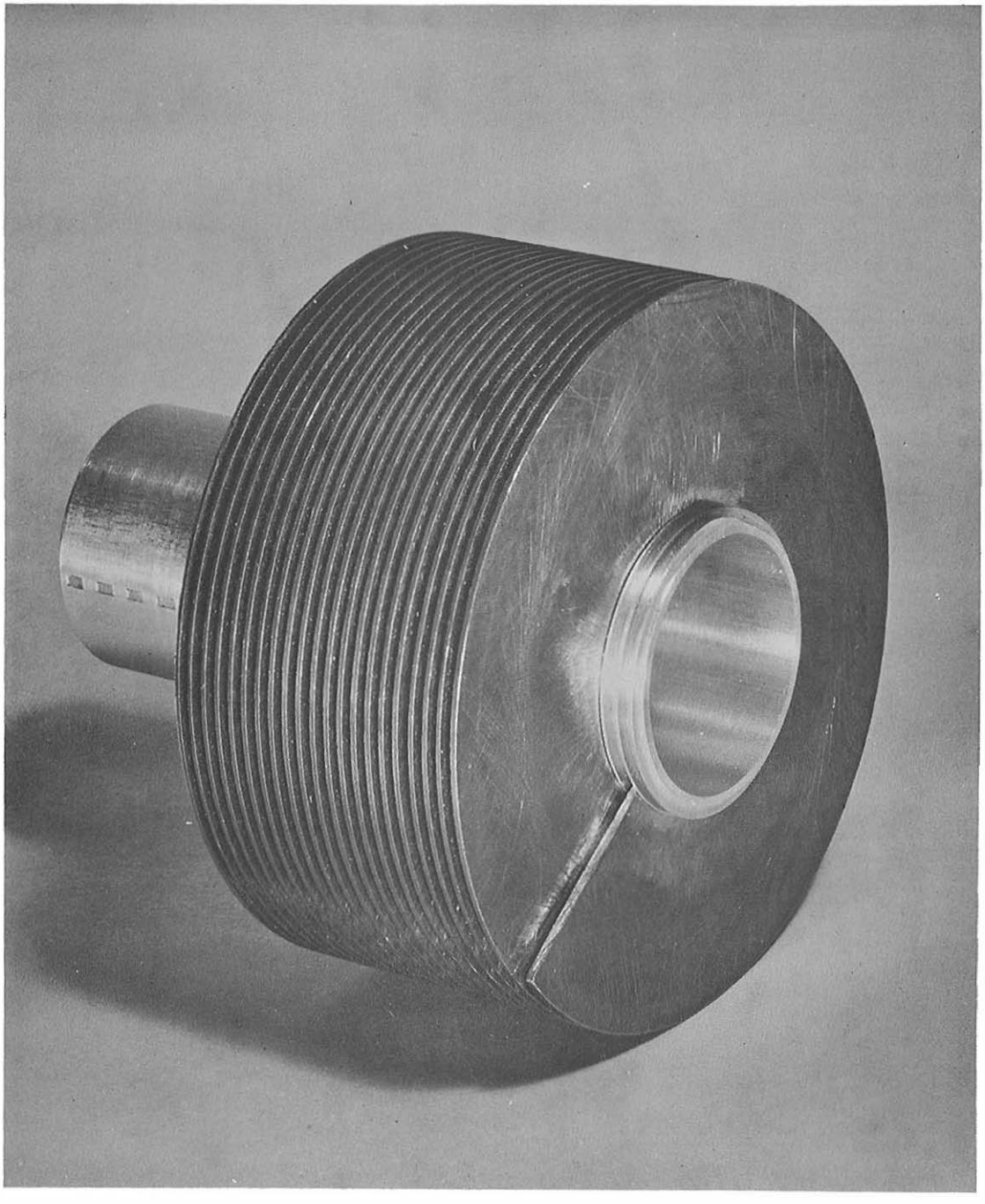

Fig. 1. Helix of Bitter Coil III on Mandrel.

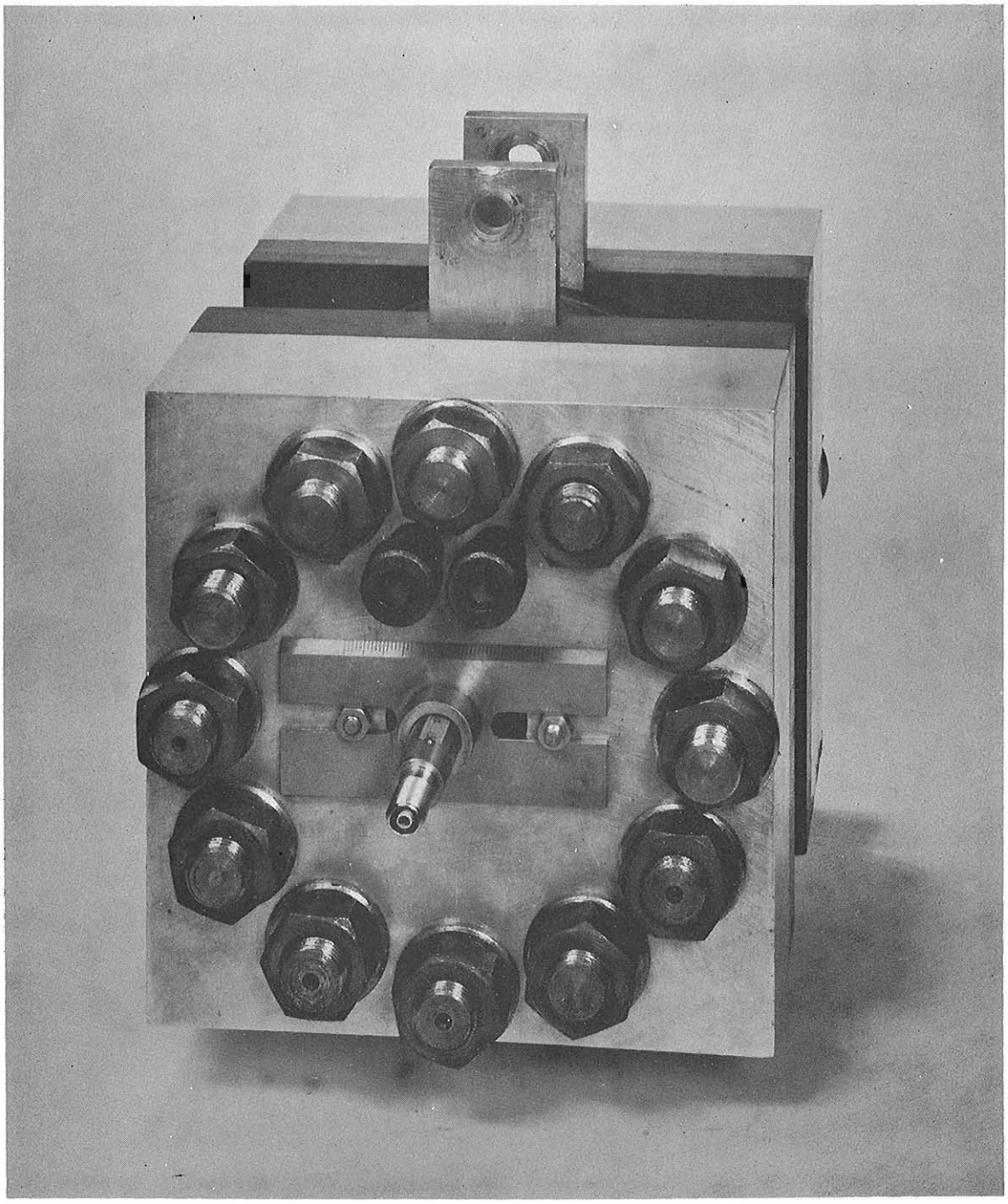

Fig. 2. Bitter Coil III between End Plates.

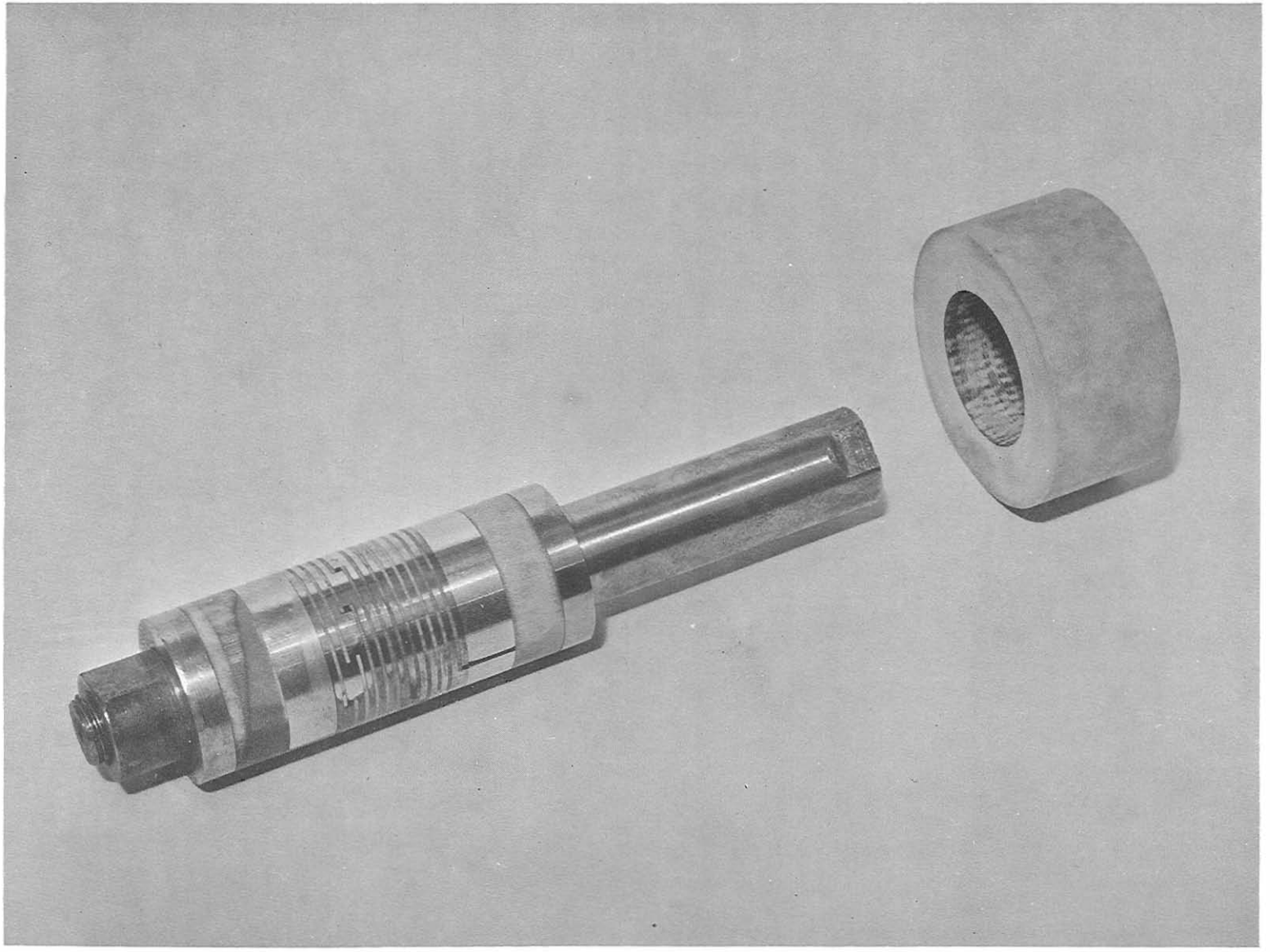

Fig. 3. Bitter Coil IV on Mandrel with Radial Compression Ring.

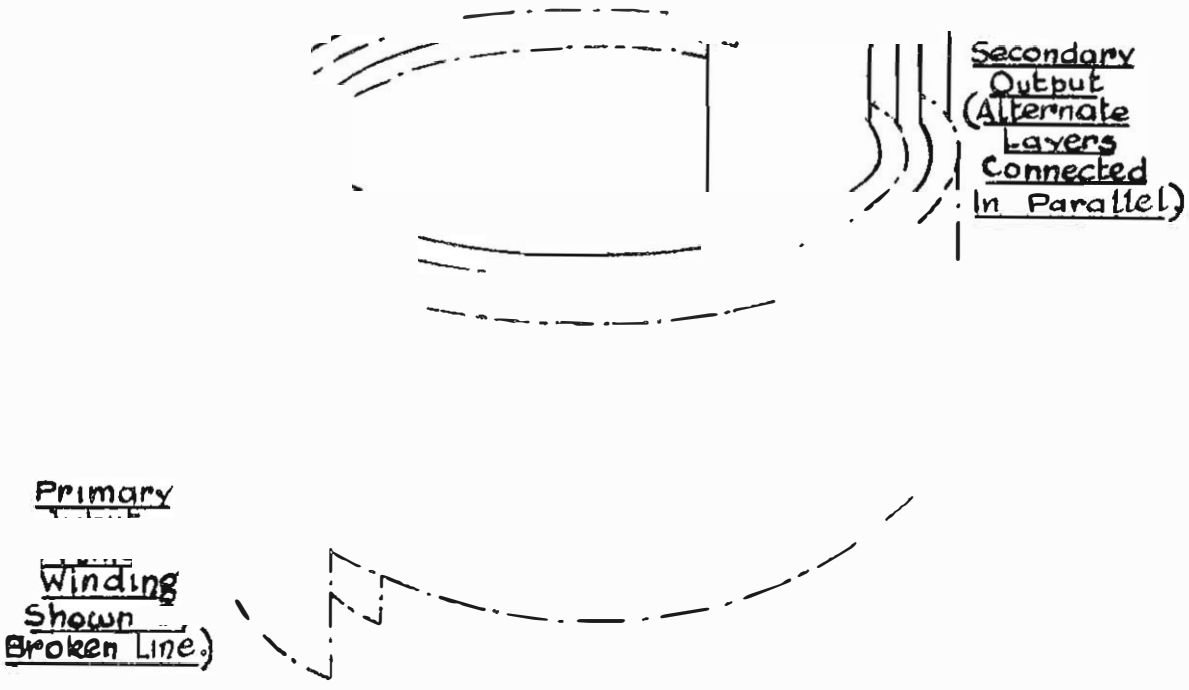

FIG. 4. THE INTERLEAVED PULSE TRANSFORMER.

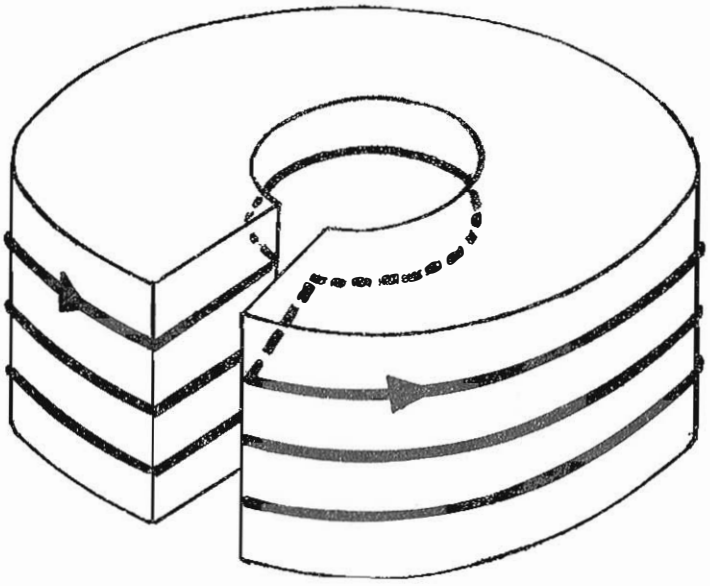

The Heavy Lines Indicate The Current Flow Induced By The Primary (Not Shown.)

FIG. 5. THE FLUX CONCENTRATOR.

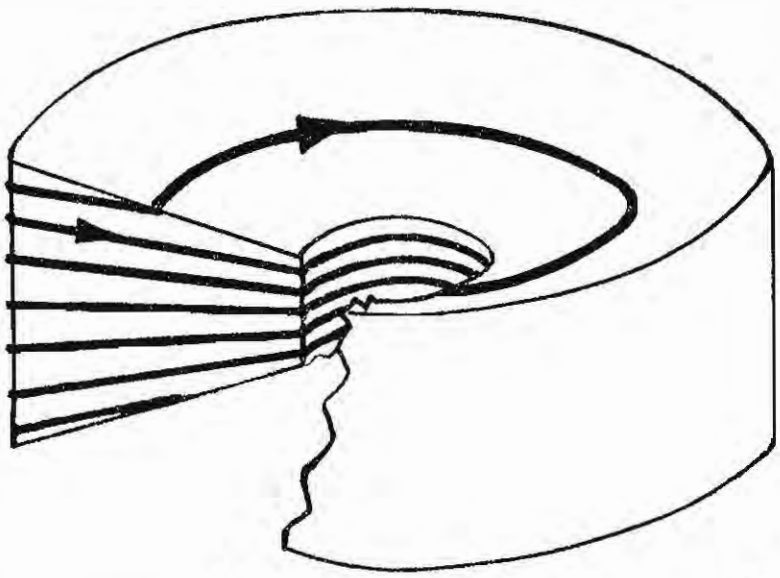

Showing The Ce Of Density The Centre And

ge

FIG. 6.

CONCENTRATOR.

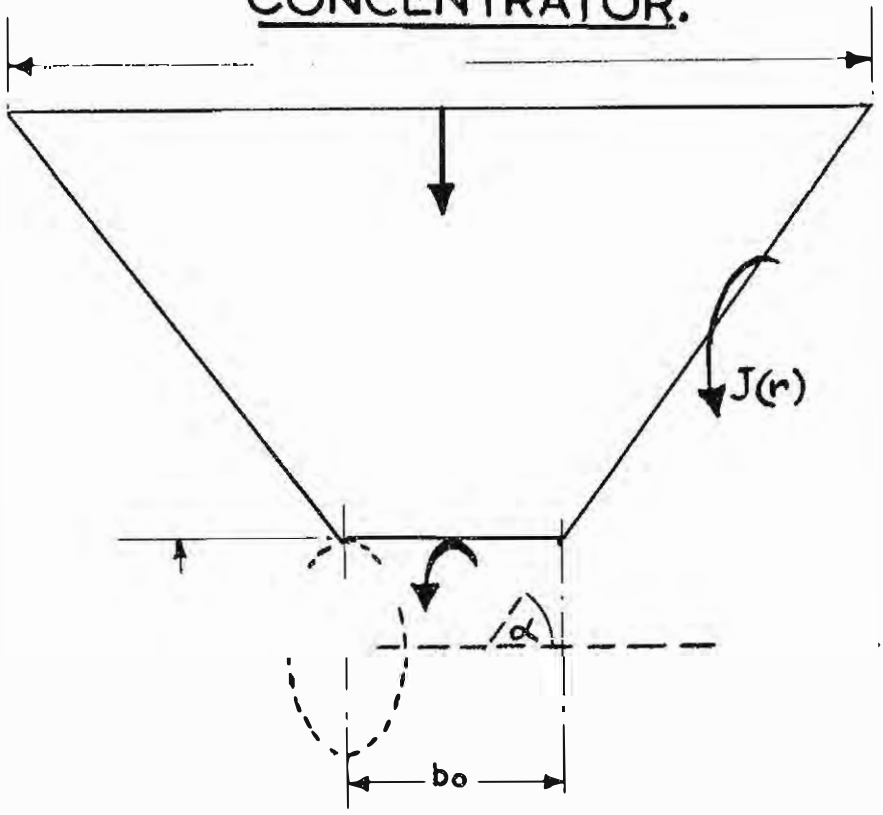

FIG. 7. TAPERED FLUX CONCENTRATOR NOMENCLATURE.

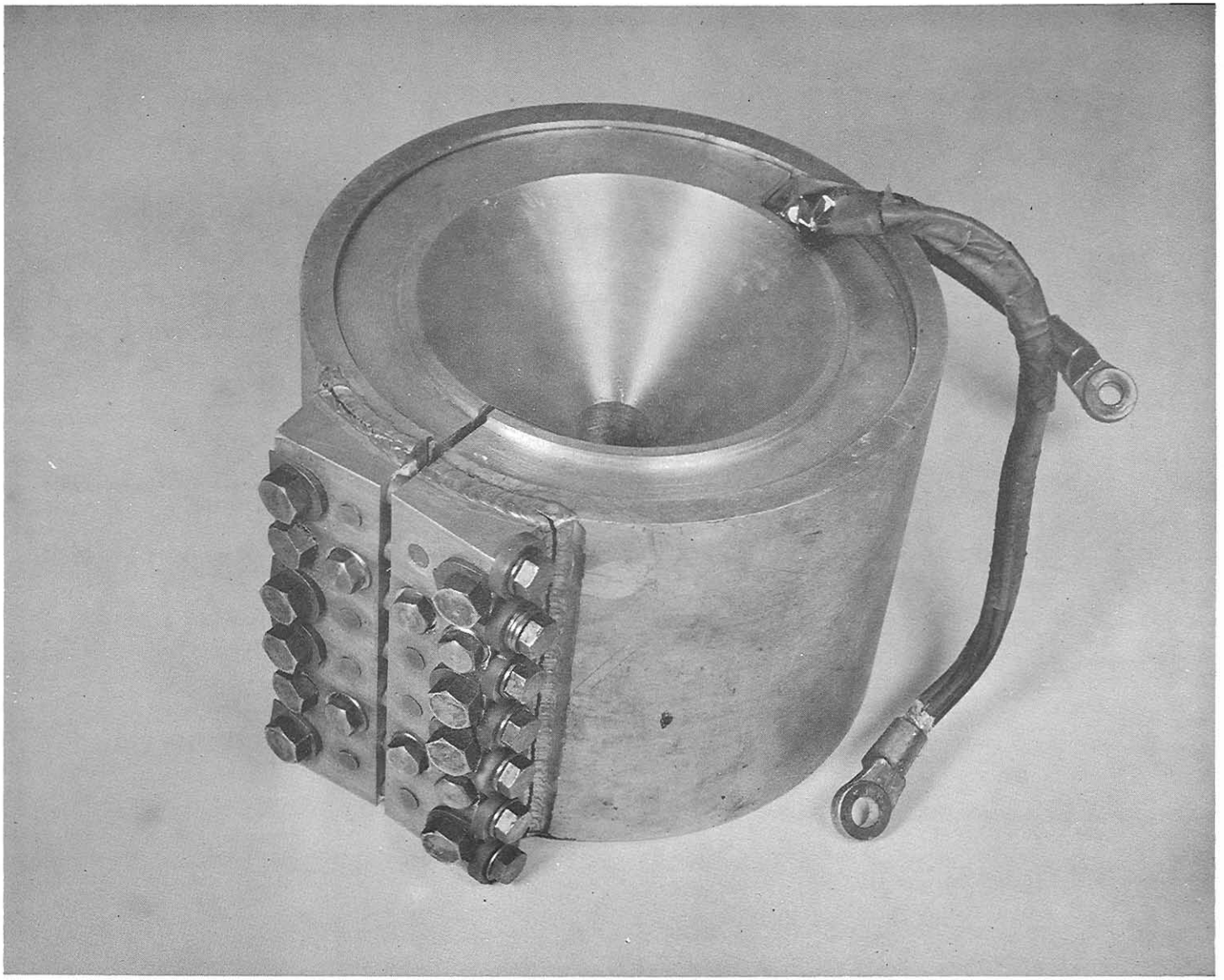

Fig. 8. Flux Concentrator No. 5.

APPENDIX 1

CAPACITOR BANK AND EXPERIMENTAL TECHNIQUES

Appendix 1(a) Capacitor Bank and Associated Equipment

The capacitor bank consists of 48 B.I.C.C. units, each of 10 μF capacity and rated at 20 kV maximum d.c. voltage. The resonant frequency of each unit is approximately 20 kc/s. The capacitors are arranged in four sections (Fig. A1.1), each with its own firing and clamping switches. The switching and clamping duties are performed by 8 ignitrons (BK24). Special care is taken to minimise the inductance and resistance in the connecting circuit, and coaxial cable (Uniradio 74) is used wherever possible. The maximum working voltage of the bank was chosen to be 13 kV; this allows a reverse voltage of up to 50 percent on oscillatory discharge. The total resistance and inductance in the discharge circuit, excluding the magnets, is estimated to be 14 milliohm and 0.58 μH, respectively. Fig. A1.2 shows a photograph of the capacitor bank and the ignitrons.

The charging circuit for the bank is a conventional full-wave rectifier circuit. The capacitor voltage is manually controlled by disconnecting the primary a.c. supply to the step-up transformer. The maximum charging voltage is 13 kV, and the charging time-constant is 20 secs. The charging unit is fully interlocked to prevent access to the capacitor bank when charged.

The triggering circuit for the ignitrons is shown in Fig. A1.3. The circuits were designed to allow any chosen time delay between the firing and clamping operations. However, for most of the experiments, simultaneous firing of the clamping and firing ignitrons was found to be adequate. The power circuit can be automatically triggered at a pre-set capacitor bank voltage by adjusting the helipot R; the manual triggering is performed by the push-button S. The above automatic trigger, along with the counter C, has proved very useful for life tests on the magnets.

Appendix 1(b) Measuring Techniques

Voltage Measurement

The voltage across the capacitor bank and across the magnet coil were measured by simple uncompensated resistance dividers. Two different resistance values for the high voltage arm were chosen: 30 MΩ for measuring the capacitor voltage (this gave a discharge time-constant of 4 hours); 100 KΩ for measuring the instantaneous voltage across the magnet coil. In both cases, the divider ratio was 1000 to 1. The dividers are completely shielded, and the high voltage input is taken through a screened coaxial cable. Grade 1 high stability resistors have been used, and the accuracy of measurement is estimated to be better than 2 per cent.

Current Measurement [19]

An independent measurement of the magnet current is necessary for accurate determination of the efficiency of any particular magnet design. A continuously rated shunt for 40 - 50 kA would be cumbersome and expensive. However, since all our magnets were intended for pulsed duty, a small coaxial shunt was designed. Fig. A1.4 shows the first design. Fig. A1.5 shows the latter design in which one terminal of the shunt was used as a common earth terminal for all measuring apparatus. This was necessary to reduce pick-up voltages due to currents in the earth loops. The resistance and inductance of these shunts have been measured on a precision ratio-arm bridge, and typical values are 1.3 milliohm and $< .01$ μH, respectively.

Field Measurement

Hall effect devices and N.M.R. probes were initially considered. However, due to the difficulty of calibrating these devices at high magnetic fields, it was decided that the best choice would be a simple search coil used with an integrator. An accuracy of better than 5 per cent was considered adequate for the present investigation. A variety of search coils were developed during the investigation and some of these are described below:

Type A - Fig. A1.6 shows the details of the search coil. The connections from the 20-turn induction coil are taken coaxially to a connector for screened cables. This construction minimises errors

due to pick-up in the connecting leads. Search coils of this type were used for measuring axial field in the experimental magnets.

Type B - Fig. A1.7 shows the details of a flat search coil which was used for measuring magnetic fields close to a current sheet (e.g. on the inner surface and inside the slot of a flux-concentrator). Since a simple relationship exists between the current density and the surface field, this search coil was very useful for estimating the current distribution in flux-concentrators.

All the search coils were used with simple C-R passive network integrators. The time-constant of these integrators ($\approx$7.5 millisec) was large compared with the magnetic field pulse duration ($\approx$0.2 millisec). The search coils along with the integrators were calibrated in a long single layer solenoid. The solenoid was energised from a stabilised variable frequency (50 c/s to 10 kC/s) source capable of delivering 10 amps. The central field in the solenoid at 10 amps. is 100 gauss. The search coil output was measured on a Tektronix oscilloscope using a Type E amplifier unit. This gives a maximum deflection sensitivity of 50 μV per cm. The accuracy of calibration is estimated to be about 2 per cent.

Appendix 1(c) Analysis of Capacitor Discharge and Clamping Circuit

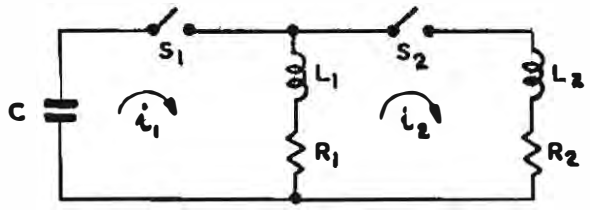

FIG. A1·8

C - Storage capacitance.

R_1, L_1 - Coil resistance and inductance.

R_2, L_2 - Clamping circuit resistance and inductance.

S_1 - Discharge initiating switch.

S_2 - Clamping switch (closes when the capacitor voltage is zero).*

i_1, i_2 - Loop currents.

Let at t=o, when S_2 is closed, the current in the magnet coil be i_o, which can be calculated from the following expression:

$$i_o = V_o w C e^{-\beta t_o} \text{ Sin } w t_o$$; where V_o is the initial capacitor voltage; $w = \sqrt{\frac{1}{L_1 C} - \frac{R_1^2}{4L_1^2}}$; $\beta = \frac{R_1}{2L_1}$; and t_o is given by the expression

$$w t_o - \tan^{-1} \frac{\beta}{w} = \frac{\pi}{2} .$$

The circuit equations when both S_1 and S_2 are closed can be transformed into two algebraic equations in terms of a complex variable s by using Laplace Transformation:

$$\begin{bmatrix} (L_1 + L_2)s + (R_1 + R_2) & -(L_2 s + R_2) \\ -(L_2 s + R_2) & \frac{1}{sC}(L_2 C s^2 + R_2 C s + 1) \end{bmatrix} \begin{bmatrix} i_1 \\ i_2 \end{bmatrix} = \begin{bmatrix} i_o L_1 \\ 0 \end{bmatrix}$$

The characteristic polynomial in s can be written as:

$$\frac{1}{sC}\,(L_2Cs^2 + R_2Cs + 1)\left\{(L_1 + L_2)s + (R_1 + R_2)\right\} - sC(L_2s + R_2)^2 = 0$$

$$\text{or, } s^3 + 2s^2(\ell + p)\,\frac{\beta}{\ell} + \frac{s}{\ell}\left\{4p\beta^2 + w_o^2\,(1 + \ell)\right\} + 2w_o^2\,\frac{\beta}{\ell}\,(1 + p) = 0$$

$$\text{where, } \ell = \frac{L_2}{L_1}\ ;\ p = \frac{R_2}{R_1} \text{ and } w_o^2 = \frac{1}{L_1C}\ .$$

A general solution of this equation is complicated; however, the condition for a non-oscillatory solution can be derived from the fact that for all real roots the discriminant of the above cubic equation must be negative. A numerical solution for specific values of ℓ, p and w_o can be readily obtained. Platner[18] has obtained analogue solution of the problem for various values of parameters ℓ and p, and has shown that the total energy dissipated in the coil can be considerably reduced by a suitable choice of ℓ and p. This consideration is very important in case of coils with moderate duty cycle and for cryogenic coils.

* The analysis becomes somewhat different in detail if S_2 is assumed to close when the current in the coil is maximum. However, in all our experiments, the ignitrons used for the switching were fired simultaneously; in this case, the current in the clamping circuit is established as soon as the capacitor voltage reverses.

APPENDIX 2

THE FORCES ACTING ON A BITTER COIL

Approximate solutions to the problem of stress in a Bitter coil may be obtained by a separate consideration of the forces in the radial direction and in the axial direction. Our approach is similar to that of ref. 7 but differs from it in detail.

Appendix 2(a) Stresses in the Radial and Azimuthal Directions

The radial distributions of current and field in an infinite solenoid are first calculated and the resulting expression for the force is then substituted into the stress equations for a disc[11]. We thus ignore end effects in the solenoid and any strength which the insulation may have in the radial direction. Solving the equation

$$\nabla^2 H - \frac{\mu}{\rho}\frac{\partial H}{\partial t} = 0$$

in cylindrical polar co-ordinates assuming H to be independent of Z and $\emptyset$ and to vary with time in a sinusoidal manner, we obtain a solution in modified Bessel functions.

$$H(r,t) = \left\{C\left(\mathrm{ber}\sqrt{\frac{2}{\delta}}\,r + j\,\mathrm{bei}\sqrt{\frac{2}{\delta}}\,r\right) + D\left(\mathrm{ker}\sqrt{\frac{2}{\delta}}\,r + j\,\mathrm{kei}\sqrt{\frac{2}{\delta}}\,r\right)\right\} e^{jwt}$$

where

w = angular frequency.

ρ = resistivity of the medium.

$\delta = \sqrt{\frac{2\rho}{w\mu}}$ = skin depth.

C, D are complex coefficients depending on the boundary conditions.

Inclusion of boundary conditions appropriate to a thick walled cylinder of inner radius r_o and approximation of the Bessel functions for the usual case of $r \gg \delta$, yields the result:-

$$H(r,t) = H_o\sqrt{\frac{r_o}{r}}\; e^{-\left(\frac{r-r_o}{\delta}\right)}\; e^{-j\left(\frac{r-r_o}{\delta} - wt\right)}$$

also the current density

$$J = \text{Curl } H = \frac{H_o}{\delta}\sqrt{\frac{2r_o}{r}}\, e^{-\left(\frac{r-r_o}{\delta}\right)}\, e^{-j\left(\frac{r-r_o}{\delta} - \frac{\pi}{4} - wt\right)}$$

Where H_o is the peak field at r_o. The force per unit volume of the conductor is given at any particular time by the product of the real parts of the two above expressions, at the peak field this is approximately

$$F(r,0) = \frac{B_o^2 r_o}{\mu \delta r}\, e^{-\left(\frac{r-r_o}{\delta}\right)}$$

Where $B_o = \mu Ho$

The two equations for the radial and azimuthal stresses in a disc, P and Q, are:-

$$\frac{\partial(Pr)}{\partial r} = Q - Fr$$

$$P - \sigma Q = \frac{\partial}{\partial r}(rQ - \sigma rP)$$

Where σ= Poisson's ratio.

Substituting the force term derived above and solving we obtain:-

$$P = F_o \left\{ K + \frac{L}{r^2} - \left(\sigma + \frac{\gamma}{2\delta}\right) \int_{r_o}^{r_1} \frac{e}{r}^{-r/\delta}\, dr + \frac{e}{2r}^{-r/\delta} \left(\frac{\gamma\delta}{r} + \gamma\right) \right\}$$

$$Q = F_o \left\{ K - \frac{L}{r^2} - \left(\sigma + \frac{\gamma}{2\delta}\right) \int_{r_o}^{r_1} \frac{e}{r}^{-r/\delta}\, dr - \frac{e}{2r}^{-r/\delta} \left(\frac{\gamma\delta}{r} + \gamma\right) \right\}$$

Where K, L are boundary condition coefficients

$$\gamma = \delta(1-\sigma)$$

$$F_o = \frac{B_o^2 r_o\, e^{r_o/\delta}}{\delta \mu \lambda}$$

λ = ratio of conductor volume to total volume of the coil ('filling factor').

r_1 = outer radius of coil.

The above expressions are independent of the scale of r to a good approximation provided that $r \gg \delta$. Figure A2.1 shows P and Q calculated for Coil III at 200 kilogauss and also a special case with K and L modified to include some radial precompression.

It should be mentioned that commonly advocated method of calculating stress in a pulsed coil by regarding the magnetic field as a gas exerting an external pressure on the conductor of $\frac{B_o^2}{2\mu}$ does not give satisfactory answers for P and Q near the inner surface although it agrees with the above calculation at points well inside the conductor.

Appendix 2(b) Stresses in the Axial Direction

Cockroft[12] has calculated the axial force on a turn of a coil by a consideration of the energy of that turn relative to the rest of the coil. We assume, to a reasonable approximation, that the current in a Bitter coil flows in a sheet at the inner surface and consider the axial force F_z on a section Δz of a turn whose total height is h.

$$F_z = \frac{\partial E_z}{\partial z} = \frac{\partial}{\partial z} \left(M_z \; i^2 \; \frac{\Delta z}{h} \right)$$

Where E_z = Energy of section Δz

M_z = Mutual inductance between the loop Δz and the coil.

i = Circulating current per turn.

The force on the complete turn is therefore:-

$$F = \frac{i^2}{h} \int_z^{z+h} \frac{\partial M_z}{\partial z} \, dz = \frac{i^2}{h} \left\{ M_{(z+h)} - M_{(z)} \right\}$$

Figure A2.2 shows this force for each turn of Coil III at 200 kilogauss, the inductances were taken from Grover[13].

Given a set of axial forces acting on the inner edge of each turn of the coil, one would now like to use this to calculate the compressive stress at all points in the insulation. This problem becomes extremely complicated in the case of a coil consisting of some 25 alternate layers of conductor and insulation and we have only attempted to make approximate estimates of the highest compressive stress in the insulator. The greatest total load is of course borne by the central layer of insulation but, because of the rigidity of the many layers of conductor, this load will be spread over a large area. From Figure A2.2 it may be seen that almost half the total force acts on the end turn and, because it all acts on the inner edge, this force will be supported by a much smaller area of insulator and the resulting stress will be high. Experimentally, it has always been found that both insulation failure and large axial deformation of the conductor occur near the ends of the coil. We therefore

calculate the stress under the end turn of the coil and assume that the coil life will be determined by this. The problem is that of an annular disc which is strong in both compression and rigidity (the conductor) supported on a compressible foundation. It is found that the height of the disc and hence the stress in the foundation vary as $\bar{e}^{\Lambda r}$ with a peak stress at the inner edge of:-

$$P = \frac{F\Lambda}{\pi r_o}$$

Where

$$\Lambda = \sqrt[4]{\frac{3Y_i}{Y_c dh^3}}$$

Y_i = Young's modulus of the foundation (insulator).
Y_c = " " " " disc (conductor).
d = Thickness of the foundation.
h = " " " disc.

This stress is again seen to be independent of the size of the coil for a given shape, number of turns etc.

Calculations for Coil III give $\Lambda = 3\ cm^{-1}$ and hence a peak stress at 200 kilogauss of 4×10^3 k.gm/cm^2. The ultimate compressive strength of the glass fibre/epoxy is estimated as about $1.0 - 2.0 \times 10^4$ k.gm/cm^2 giving a failure field of 300 - 400 kilogauss.

APPENDIX 3

TRANSFORMER COIL THEORY

Appendix 3(a) Circuit Relations and Efficiency

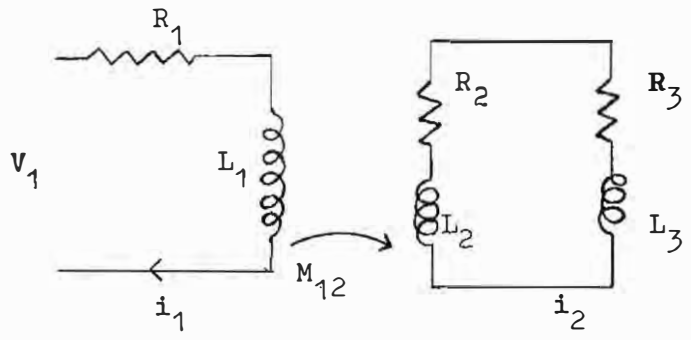

We represent a transformer coil by the above lumped circuit in which the variables subscripted 1, 2 and 3 refer to the primary, secondary and single turn load respectively. The response of the circuit to a sinusoidally varying voltage across the primary is governed by the following equations.

$$V_1 = i_1R_1 + jwL_1i_1 - jwM_{12}i_2 + jwM_{13}i_2$$

$$0 = jwL_2i_2 + jwL_3i_2 - 2M_{23}jwi_2 + i_2(R_2 + R_3) + jwM_{13}i_1 - jwM_{12}i_1$$

$$\therefore i_2 = \frac{jwi_1 (M_{12} - M_{13})}{(R_2 + R_3) + jw(L_2 + L_3 - 2M_{23})}$$

$$= jwi_1 \frac{(M_{12} - M_{13}) (R_2 + R_3) - w^2 (M_{12} - M_{13}) (L_2 + L_3 - 2M_{23})}{(R_2 + R_3)^2 - w^2 (L_2 + L_3 - 2M_{23})^2}$$

Substituting into the first equation:-

$$V_1 = i_1 \left\{ R_1 + \frac{w^2 (M_{12} - M_{13})^2 (R_2 + R_3)}{(R_2 + R_3)^2 - w^2 (L_2 + L_3 - 2M_{23})^2} \right\}$$

$$+ \; jwi_1 \left\{ L_1 - \frac{w^2(M_{12} - M_{13})^2 (L_2 + L_3 - 2M_{23})}{(R_2 + R_3)^2 - w^2 (L_2 + L_3 - 2M_{23})^2} \right\}$$

The transformer therefore behaves as a circuit element of resistance R_p and inductance L_p given by the terms in the brackets. In practice we normally find:-

$$w(L_2 + L_3 - 2M_{23}) \gg R_2 + R_3$$

$$L_2 = n^2 L_1 \qquad \text{where n is the number of primary turns}$$

$$M_{13} = nM_{23}$$

A coupling coefficient between primary and secondary is defined by

$$k^2 = \frac{M_{12}^2}{L_1 L_2} = \frac{M_{12}^2}{n^2 L_2^2}$$

$$i_2 \simeq \frac{(M_{12} - M_{13})i_1}{L_2 + L_3 - 2M_{23}} = \frac{n(kL_2 - M_{23})}{L_2 + L_3 - 2M_{23}} i_1$$

Let $\ell = L_2/L_3$ and $m = M_{23}/L_3$

$$i_2 = \frac{n(k\ell - m)}{(\ell + 1 - 2m)}$$

$$R_p = R_1 + (R_2 + R_3) n^2 \left\{ \frac{k\ell - m}{\ell + 1 - 2m} \right\}^2$$

$$L_p = L_1 - n^2 \frac{(k\ell - m)^2}{\ell + 1 - 2m} = n^2 L_3 \left\{ \ell - \frac{(k\ell - m)^2}{\ell + 1 - 2m} \right\} \simeq n^2 L_3$$

If the load is short circuited, i.e., $R_3 = L_3 \simeq 0$ we have:-

$$R_p' = R_1 + k^2 n^2 R_2$$

$$L_p' = L_1 (1 - k^2)$$

The resistive energy dissipation in the circuit before the first current maximum, E_R and the inductive energy stored in the circuit at the current maximum are:-

$$E_R = \frac{\pi}{w} \left\{ i_1^2 R_1 + i_2^2 (R_2 + R_3) \right\} = \frac{\pi}{w} i_1^2 R_p$$

$$E_L = \frac{1}{2} L_1 i_1^2 + \frac{1}{2} (L_2 + L_3) i_2^2 - (M_{12} - M_{13}) i_1 i_2 - M_{23} i_2^2$$

$$= \frac{1}{2} L_p i_1^2$$

The inductive transfer efficiency is therefore:-

$$\epsilon_L = \frac{\frac{1}{2} L_3 i_2^2}{\frac{1}{2} L_p i_1^2} \simeq \frac{(k\ell - m)^2}{(\ell + 1 - 2m) \left\{ \ell (\ell + 1 - 2m) - (k\ell - m)^2 \right\}}$$

This function in the region of practical interest has the general form of Figure A3.1 which is plotted for the particular case of $m = 0$ and $k = 0.98$. In Figure A3.2 we consider the more general case and plot the maximum value of ϵ_L with respect to for all useful values of k and m.

Appendix 3(b) Coupling Measurements on Transformer Coils

It was shown in Appendix 3(a) that the coupling coefficient of a transformer coil can be estimated by measuring the primary impedance with the secondary open-circuited and short-circuited. The coupling coefficient in terms of these measured values is given as $k = \sqrt{1 - \frac{L'_p}{L_1}}$

In order to assess the effect of helical groove parameters on coupling for a flux-concentrator, a series of experiments was carried out for varying groove depth, pitch and frequency. The width of the groove was held constant at 3.175 mm. Primary winding impedance, without the metal slug, was measured by using an insulating fibreglass former. The short-circuited secondary condition was simulated by using a metal (Dural) former with an identical winding groove and with no radial slot or central hole. The measurements were repeated at various supply frequencies. The primary winding was either 2.54 x 2.54 mm copper wire with cotton insulation or rubber insulated power cable (Unipren 12) with an overall diameter of 3.3 mm and conductor area of 0.0116 sq.cm. All the measurements were carried out with a Universal ratio-arm bridge. The broad conclusions of this investigation are summarised below:

1. The effect of altering the pitch of the helical groove on coupling is shown in Figure A3.3. The smaller the pitch the better the coupling. If the width of the ridge between grooves is of the order of twice the skin depth, the coupling is expected to be better, since more current is forced to flow closer to the surface of the groove.

2. For a given pitch and width of groove, the coupling improves with frequency, and with the depth of winding (Figures A3.4 and A3.6).

3. For a given groove dimension, coupling is better for 2.54 x 2.54 mm copper primary than for rubber insulated power cable (Unipren 12); the coupling in the latter case is approximately equal to that obtained with 2.54 x 2.54 mm copper of equivalent conductor depth in the helical groove.

It is possible to arrive at a theoretical estimate of the coupling by calculating the leakage inductance between the primary and secondary current sheets. The equivalent circuit of a transformer can be re-drawn as shown in Figure A3.5 below:

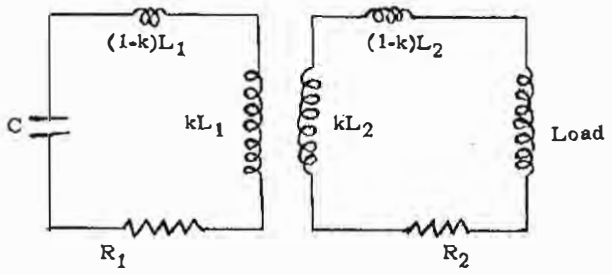

FIG. A3.5

The leakage inductance thus calculated can be equated to $(1-k)L_1$, since in the case of flux-concentrators most of the leakage flux is confined between the primary and secondary current sheets in the helical groove. Inductance between two current sheets is given by the expression:

$$L = \frac{\mu_o \cdot \ell_s \cdot w}{d} \quad \text{Henries,}$$

where ℓ_s is the length, d is the width, and w is the separation between the sheets, and μ_o is the permeability of free space. In the case of a helical groove of n turns, depth d_s, width w_s and thickness of insulation w_i, the above expression becomes:

$$\text{Leakage inductance} = L_1(1-k) = \frac{\mu_o \, 2\pi n(a_1 - d_s)(w_i + 2\delta)}{(2d_s - 2w_i + w_s)} \quad \text{Henries.}$$

Where a_1 is the outside radius of the concentrator, δ is the skin depth, and the primary and secondary currents are assumed to flow at one skin depth below the surface. Figure A3.6 shows the calculated and measured values of coupling for an experimental flux-concentrator at two values of the supply frequency. The calculated results are somewhat pessimistic due to the assumption made about the current flow.

Using the above expressions, it is possible to estimate the expected improvement in coupling for an interleaved transformer coil discussed in section 3.3.

Appendix 3(c) Currents on the Inner Surface of the Slug

An approximate solution for distribution of current on the inner surface of a tapered slug (Figure 6) may be obtained by combining the solutions for the field inside a conducting cone and a conducting cylinder. End effects and axial assymetry due to the slot are ignored and the cone and cylinder are assumed to enclose the same total flux.

Solving $\nabla^2 A = 0$ in cylindrical co-ordinates and with a conducting conical boundary at $\theta = \alpha$ we have:-

$$A_r = A_\theta = 0$$

$$A_\phi = \frac{N\ (\text{Cosec}\ \theta - \text{Cot}\ \theta)}{2\pi r^2\ (1 - \text{Cos}\alpha)}$$

$$\therefore\ B_r = \text{Curl}_r A = \frac{N}{2\pi r^2\ (1 - \text{Cos}\alpha)}$$

When N = Total flux enclosed.

For a cylindrical boundary of radius a_o and carrying a surface current density J_o we have

$$N = \mu\pi\ a_o^2 J_o$$

$$B_r = \mu\pi \frac{a_o^2 J_o}{2\pi r^2\ (1-\text{Cos}\ \alpha)}$$

The surface density at some point r on the conical boundary (Figure 7) is therefore

$$J(r) = \frac{a_o^2 J_o}{2r^2\ (1-\text{Cos}\alpha)}$$

The total current circulating on the two end faces is thus

$$I\ (\text{end}) = 2\int_{r_o}^{r_1} J(r)\,dr = \frac{a_o^2 J_o}{1 - \cos\alpha}\int_{r_o}^{r_1} \frac{dr}{r^2}$$

$$\simeq \frac{a_o J_o \sin\alpha}{1 - \cos\alpha}$$

When the outer radial distance $r_1 \gg$ inner r_o

In Figure A3.7 we plot this function together with the experimental points obtained from surface current measurements made with the flat search coil described in Appendix 1.

The total current entering the slot from the slug outer surface is:-

$$I_1 = I_o + I\ (\text{end}) = J_o \left\{ b_o + \frac{a_o \sin\alpha}{1 - \cos\alpha} \right\}$$

A current concentration factor, U, may be defined as the ratio of the inner and outer surface current densities.

$$U = J_o/J_1 = \frac{b_1}{b_o + \dfrac{a_o \sin\alpha}{1 - \cos\alpha}}$$

This factor may be used to calculate the force on the primary and bursting force on the slug as a function of the central field.

The apparent inductance of the whole inner region as seen from the outer edge of the slot is approximately (ignoring the self inductance of the slot):-

$$L_3' = L_3 \left(\frac{I_o}{I_1}\right) = L_3 \left\{ \frac{b_o}{b_o + \dfrac{a_o \sin\alpha}{1 - \cos\alpha}} \right\}$$

The efficiency is therefore reduced to :-

$$\epsilon'_L = \epsilon_L \left(\frac{L'_3}{L_3} \right) = \epsilon_L \left\{ \frac{b_o}{b_o + \frac{a_o \sin \alpha}{1 - \cos \alpha}} \right\}$$

Appendix 3(d) Calculation of Stresses in a Flux-concentrator

A simple method of estimating the mechanical strength of a flux-concentrator, with conical inside geometry (Figure 7), is outlined below. The method is based on curved-bar derivations due to Timoshenko[20].

For a bar of constant cross-section subjected to pure bending, due to couples M applied at the ends, the maximum tensile stress, Q_o, is given by

$$Q_o = \frac{M}{A} \frac{(h_1 - e)}{ea_o}$$

Where, e is a function of the geometry of the cross-section,

A = cross-sectional area,

r = radius of the centroid axis, and

h_1 = distance at the centroid axis from the inner edge.

In the case of trapezium shaped section, the value of e is given by the expression:

$$e = r \cdot \frac{m}{m + 1} \quad , \text{ where,}$$

$$m = \frac{r}{A} \left[\left\{ b_o - a_o \frac{(b_1 - b_o)}{h} \right\} \log_e \frac{a_1}{a_o} + (b_1 - b_o) \right] - 1$$

Forces acting on a flux-concentrator are:

(a) Magnetic pressure P_1, acting on the inner surface of the concentrator. This gives rise to a total force F_1 acting across the axis.

(b) Magnetic pressure inside the slot gives rise to a force F_2; this force varies with the radius depending upon the degree of current concentration, U (Appendix 3(c).

The magnetic pressure P_1 is approximately equal to $B^2/2\mu$. In most practical cases the bending moment due to F_2 is much larger than that due to F_1. In the following calculations, therefore, the contribution to F_1 from the conical end-sections is neglected.

The centre of gravity of the trapezoidal section is at a distance $h_1 = \frac{h}{3} \cdot \frac{(b_o + 2b_1)}{(b_o + b_1)}$ from the inner surface.

The magnetic pressure in the slot at the inner radius, a_o, is P_1. If the current concentration is U, the magnetic pressure in the slot at the outer radius, a_1, is approximately P_1/U^2. Assuming the magnetic pressure to vary linearly from the inside to the outside edge of the slot*, the total force F_2 acting in the slot is given by:

$$F_2 = P_1 \cdot \frac{h}{6} \cdot \left\{ \frac{(b_o + 2b_o)}{U^2} + (b_1 + 3b_o) \right\}$$

and the centre of gravity of this force is at a distance y_o from the inner surface, where

$$y_o = \frac{h}{2} \cdot \left\{ \frac{U^2(b_1 + 2b_o) + (b_o + 3b_1)}{U^2(b_1 + 3b_o) + (b_o + 2b_1)} \right\}$$

The force F_1 on the other hand, is given by:

$$F_1 = 2P_1 \cdot a_o \cdot b_o$$

The bending moments due to these forces across the cross-section are:

$$M_1 = F_1(a_o + h_1) \; ; \; M_2 = F_2(y_o + 2a_o + h_1)$$

$$M = M_1 + M_2$$

The above value of M has been used in the expression for Q_o to determine the safe working magnetic field for the flux-concentrator 6 (Table II). This field is calculated to be approximately 145 kilogauss.

* This gives a pessimistic estimate of the strength of the concentrator, since the magnetic pressure in the slot decreases somewhat more rapidly away from the inner edge.

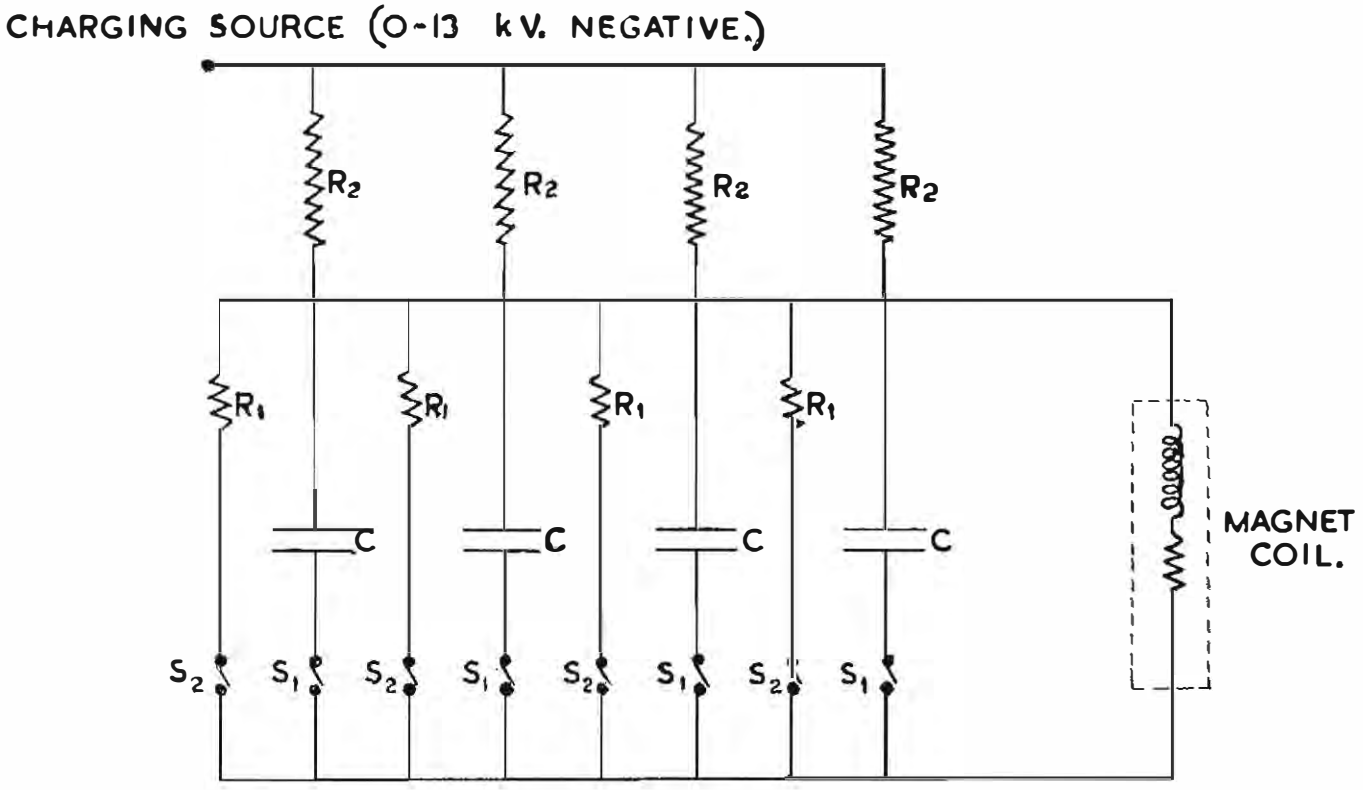

C - CAPACITOR BANK SECTIONS: 120 μF.

R_1 - CLAMPING RESISTORS: 0·1Ω.

R_2 - CHARGING RESISTORS: 180kΩ

S_1 - DISCHARGE INITIATING IGNITRONS: Bk.24.

S_2 - CLAMPING IGNITRONS: Bk 24.

CONNECTING CO-AXIAL CABLE: UNIRADIO 74.

FIG. A1·1. CAPACITOR BANK.

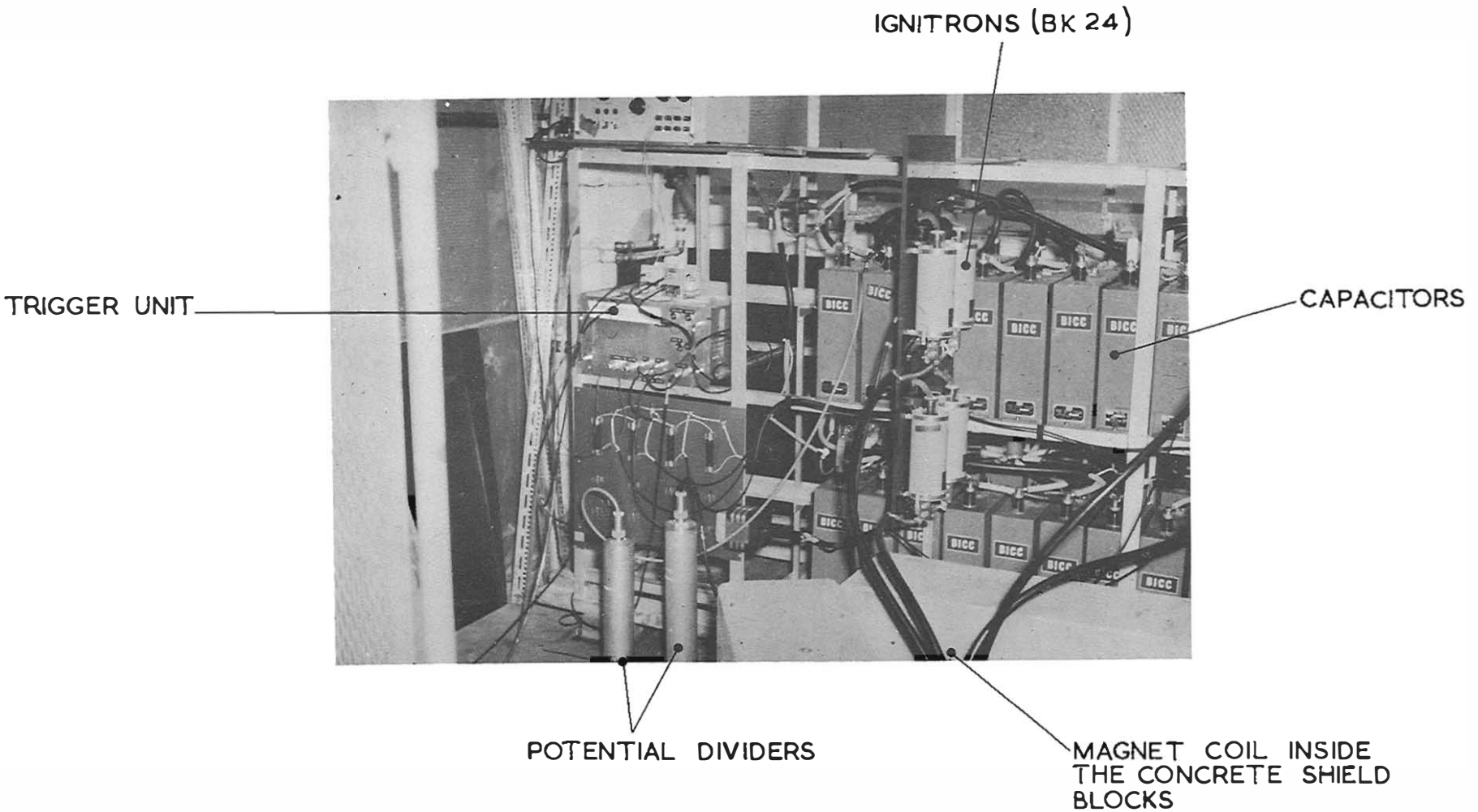

Fig. A1.2. Capacitor Bank and Associated Equipment.

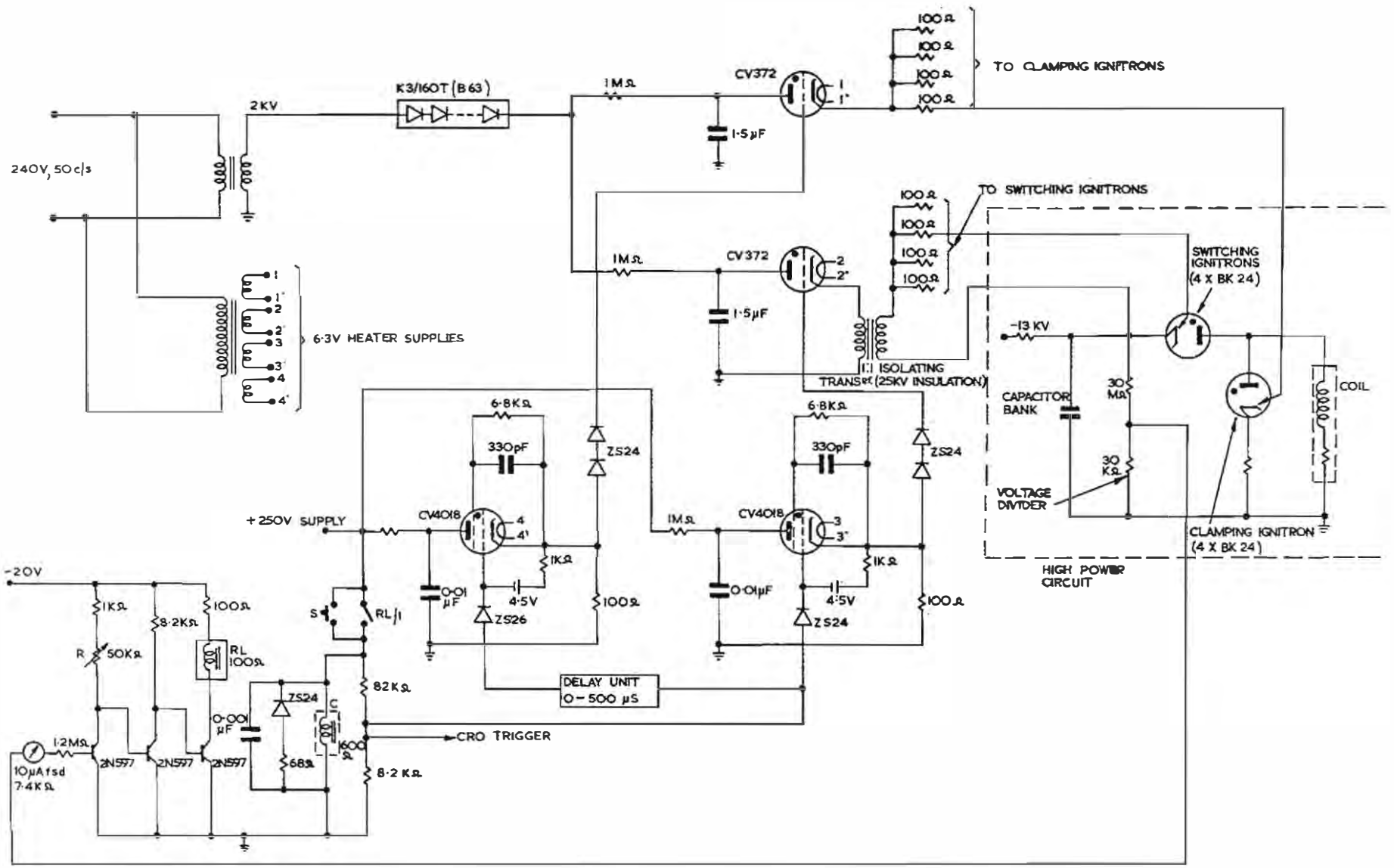

FIGURE A1·3 CONTROL CIRCUIT FOR IGNITRONS

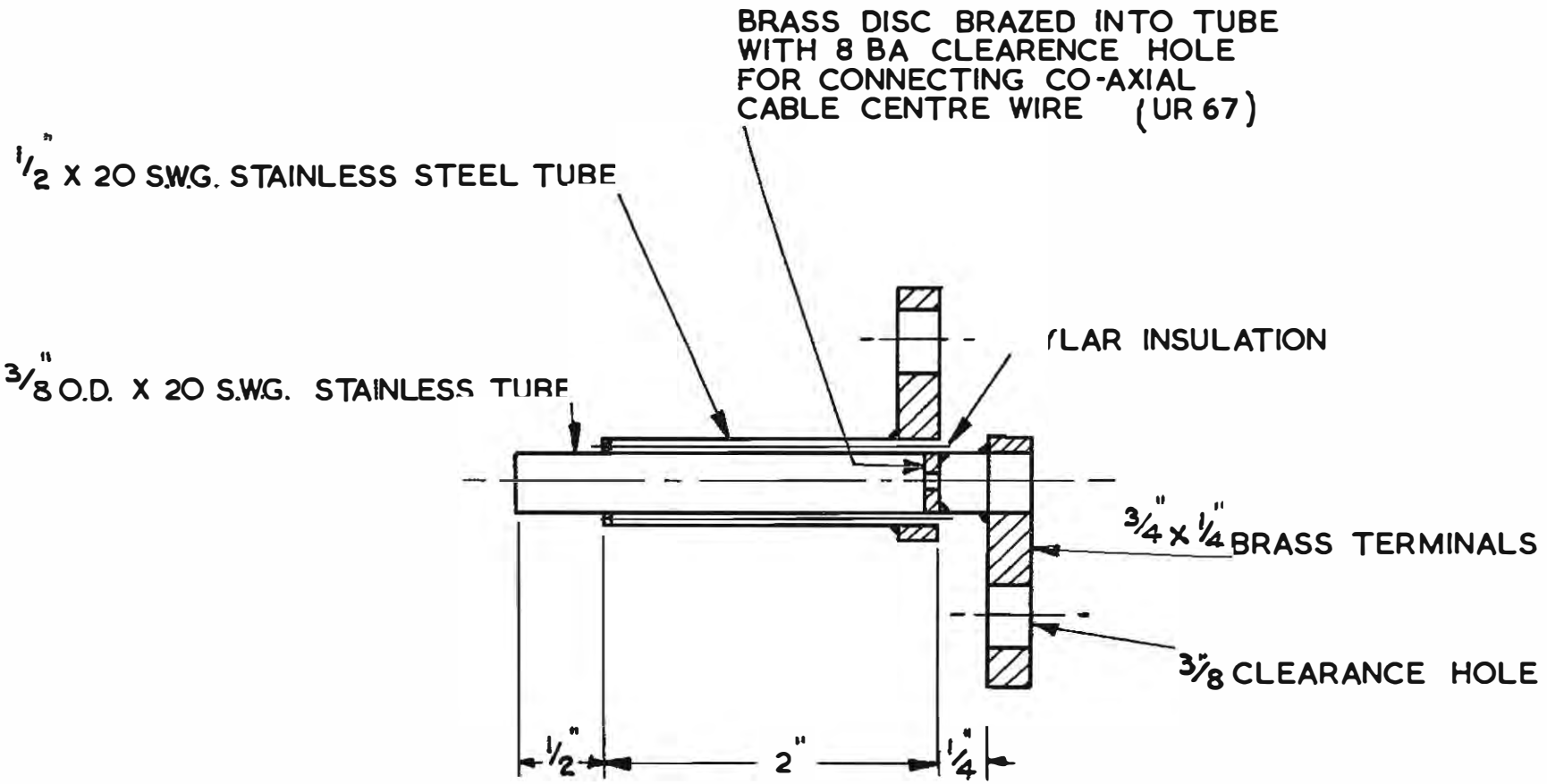

$R = 1{\cdot}2\,m\Omega$, $L << 0{\cdot}001\,\mu H$

FIGURE A1·4 COAXIAL SHUNT

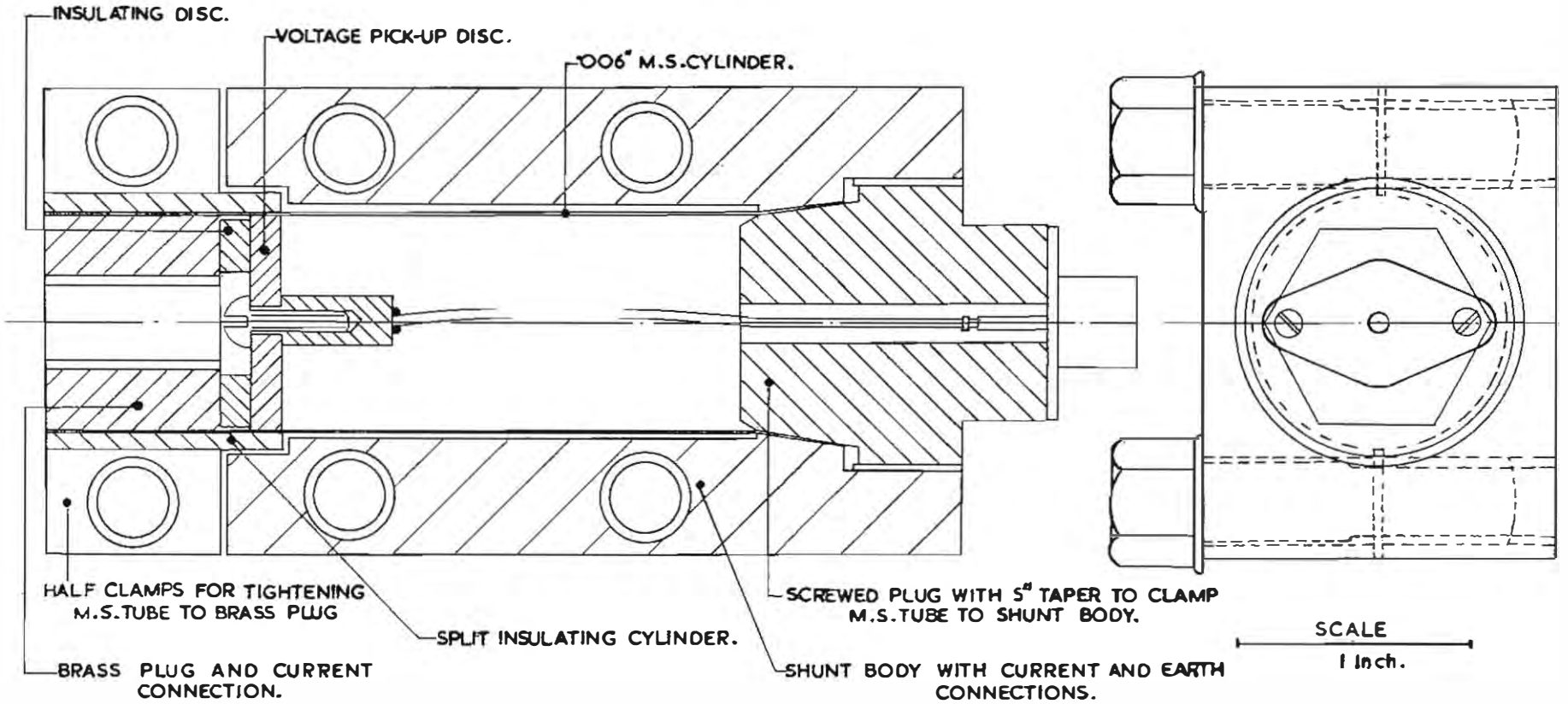

M.S.TUBE MADE BY ROLLING ·006" FOIL

FIG. A1·5. COAXIAL SHUNT AND TERMINAL BLOCK.

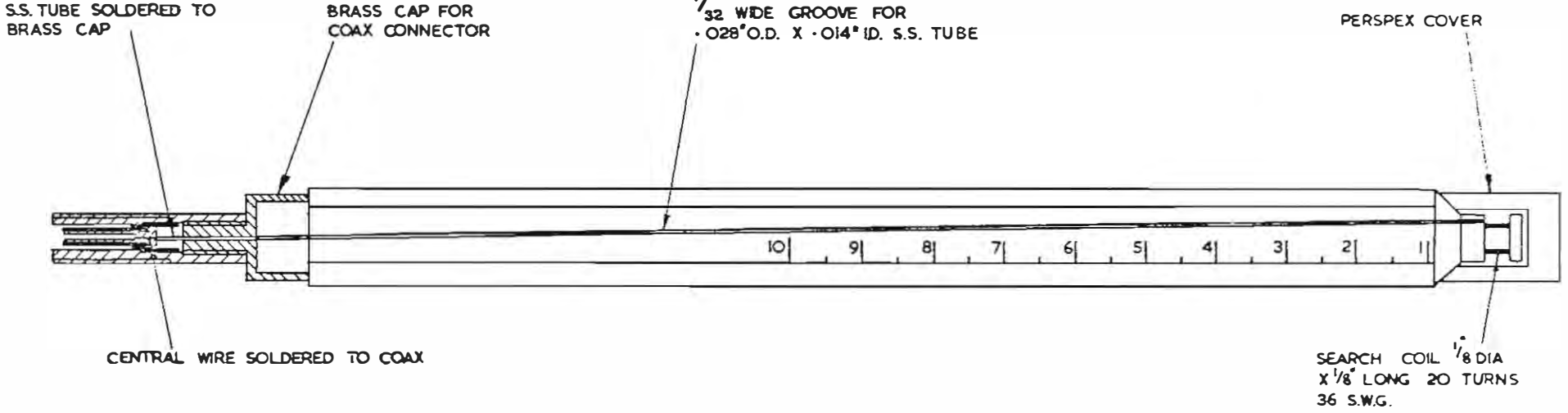

FIGURE A1·6 SEARCH COIL TYPE A

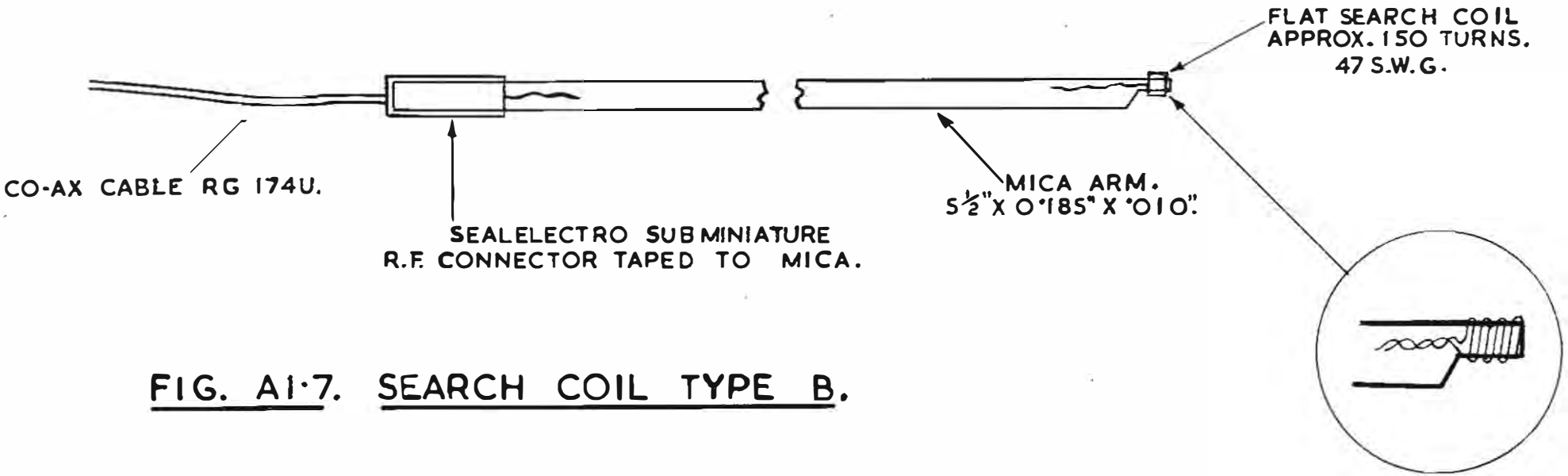

FIG. A1·7. SEARCH COIL TYPE B.

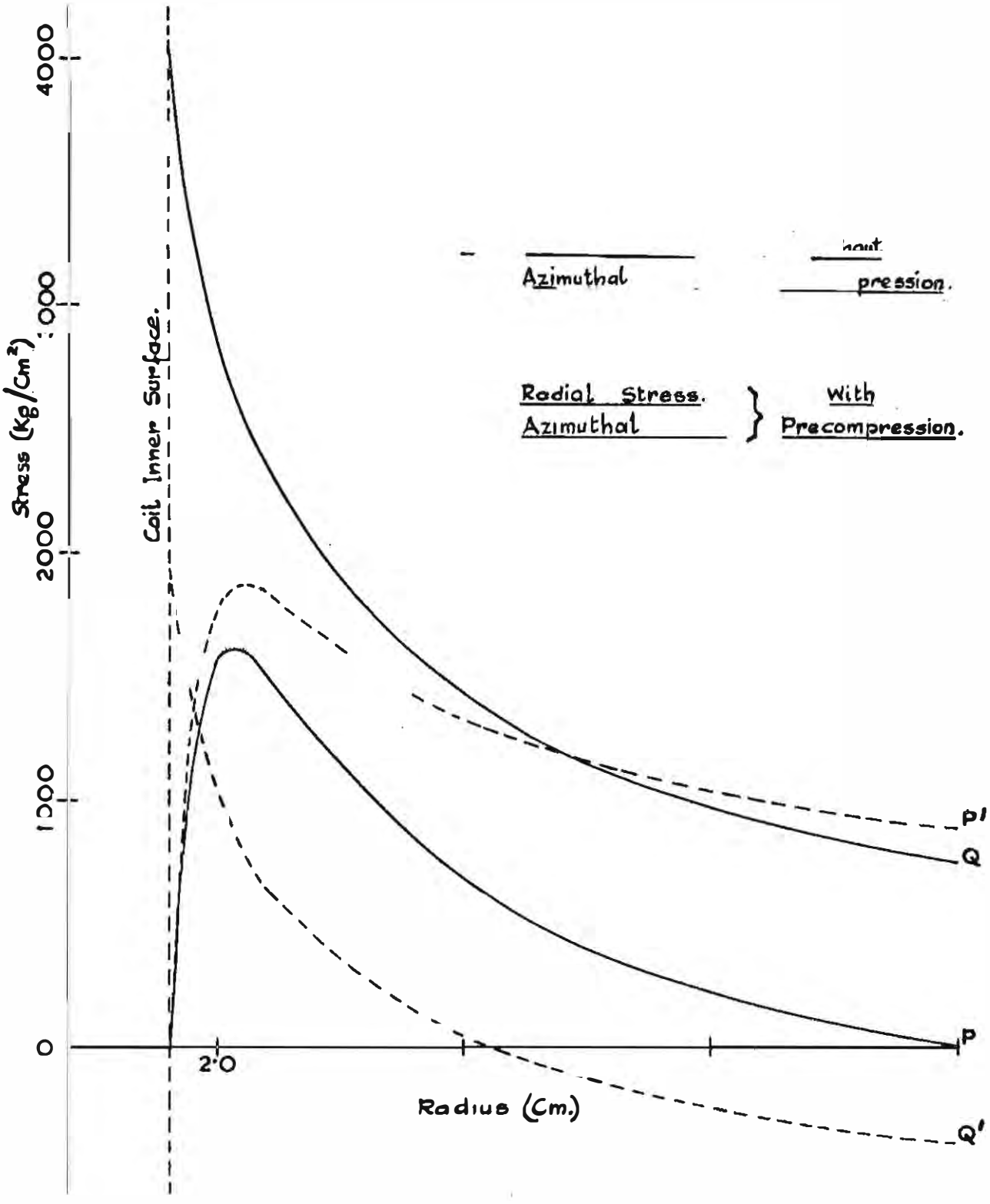

FIG. RADIAL

IN BITTER COIL III.

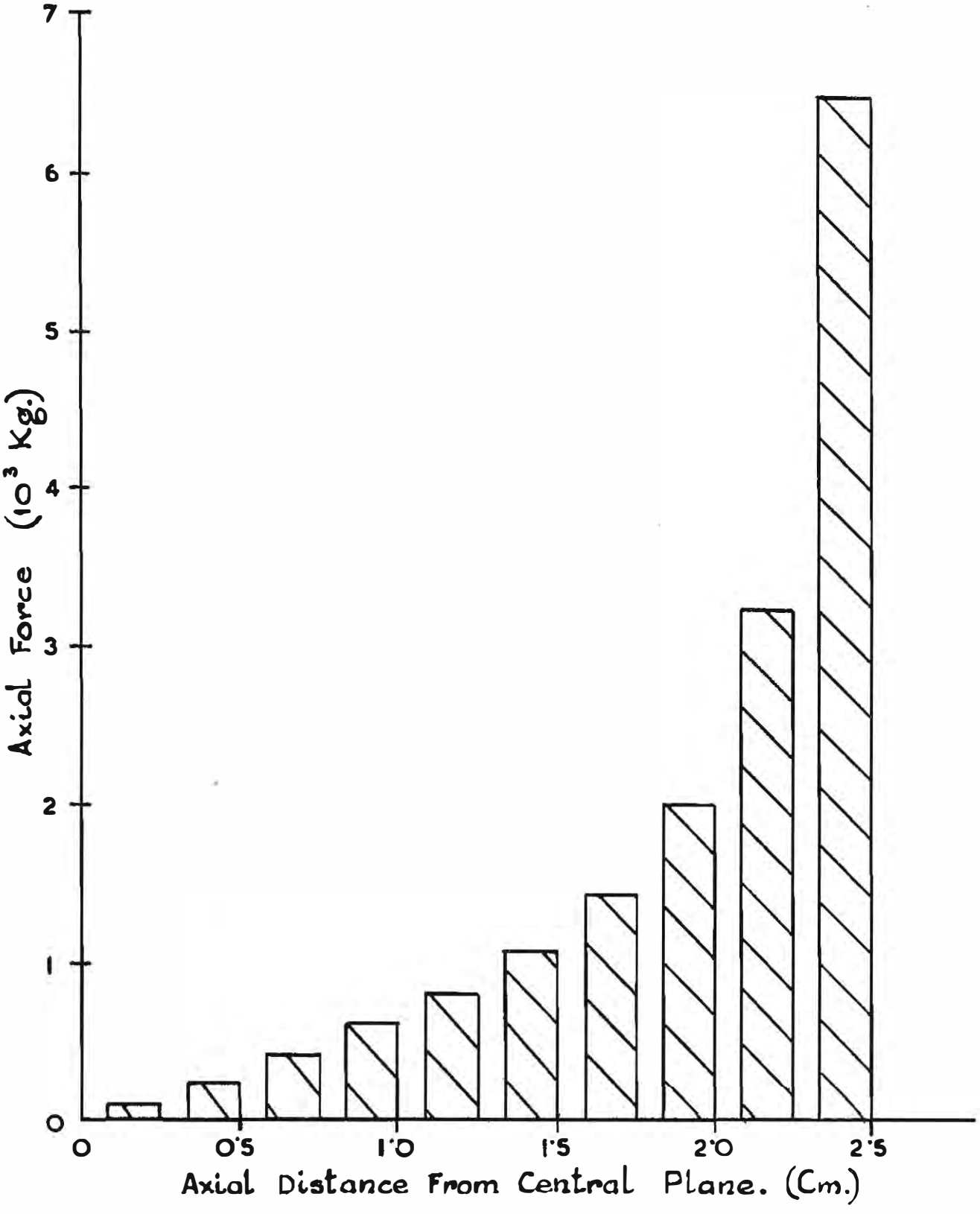

FIG.A 2·2. AXIAL FORCE ON EACH TURN OF BITTER COIL III AT 200 KILOGAUSS.

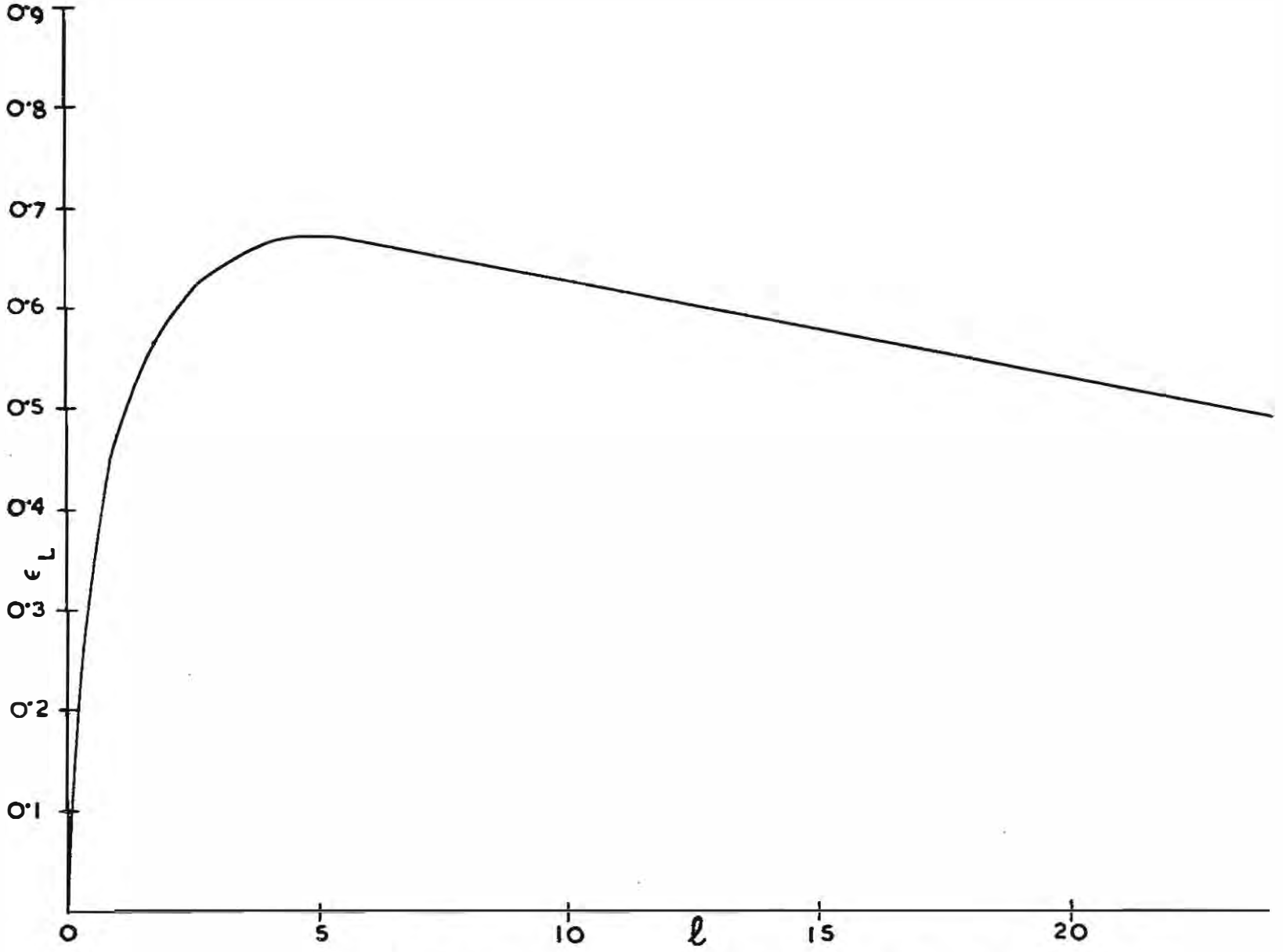

FIG. A 3·1. VARIATION OF INDUCTIVE EFFICIENCY WITH 'ℓ'

($k = 0{\cdot}98$ $M = 0$)

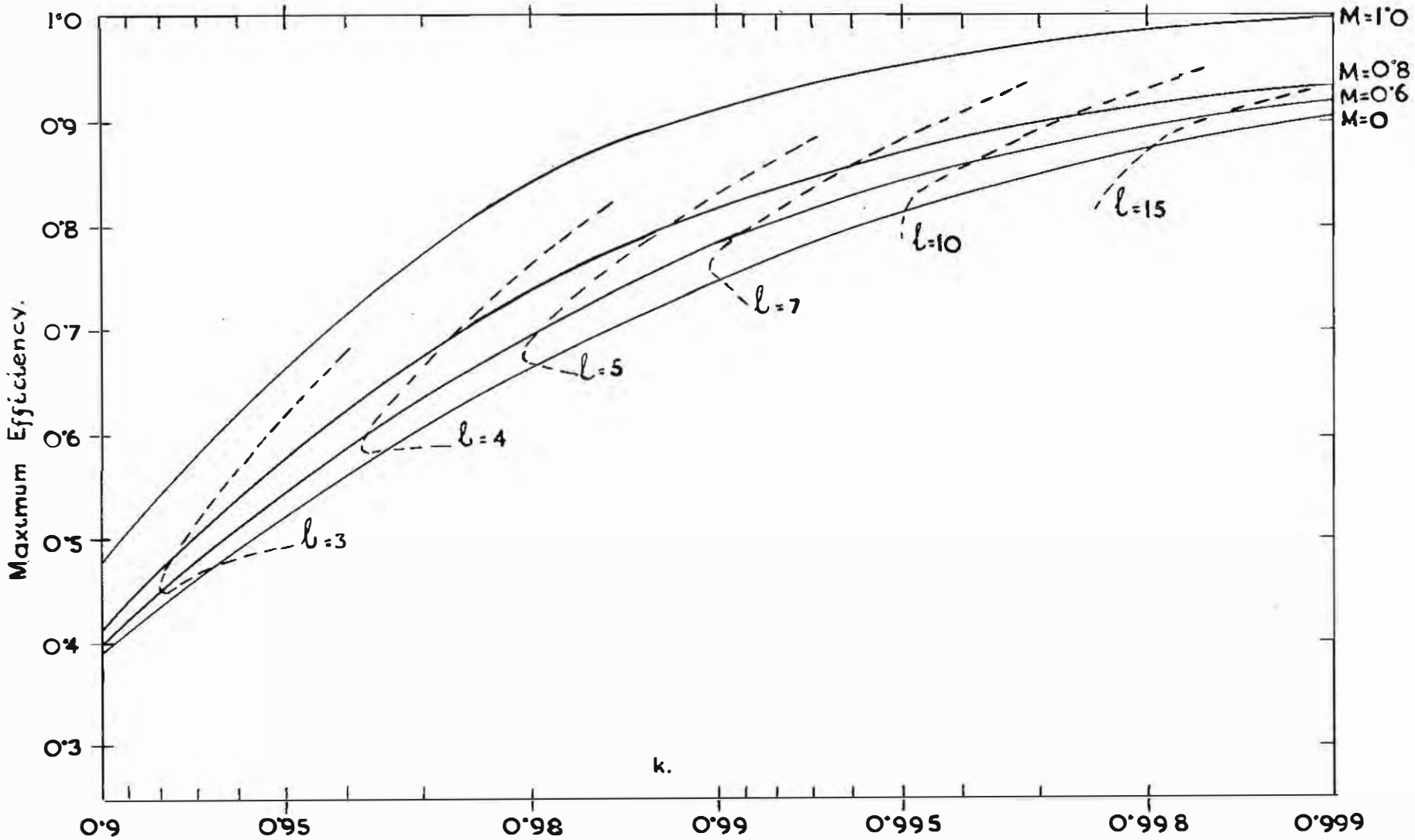

FIG. A3·2. MAXIMUM EFFICIENCY OF TRANSFORMER COILS.

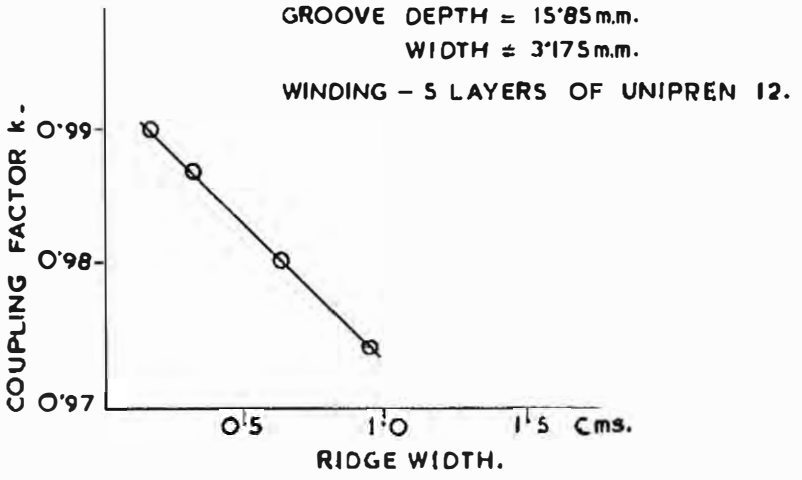

FIG. A3·3. VARIATION OF COUPLING WITH RIDGE WIDTH.

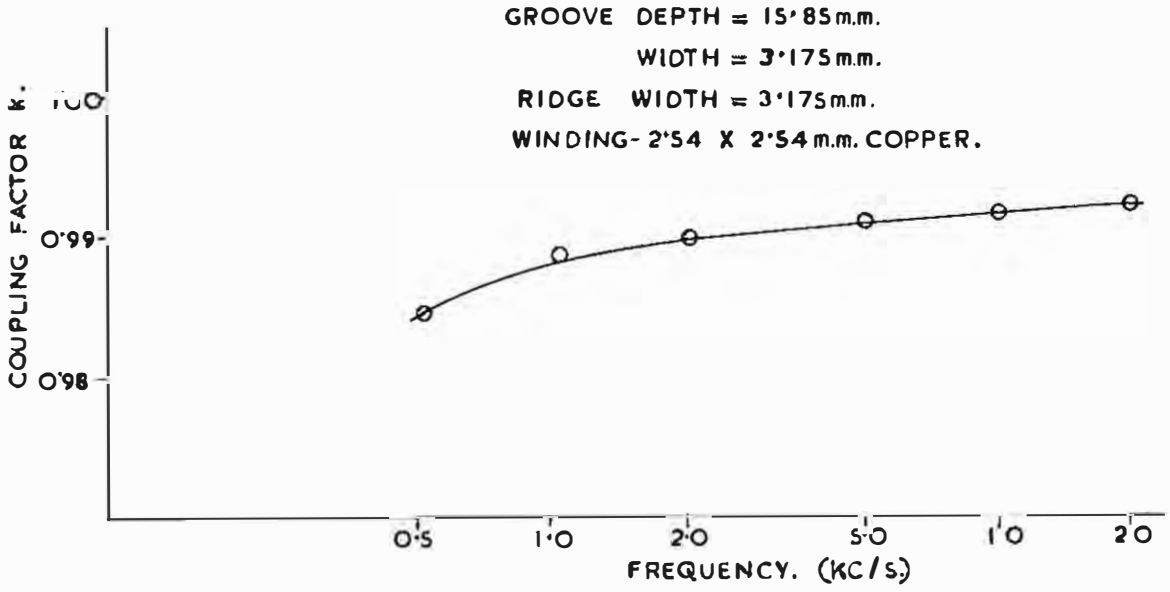

FIG. A3·4. V FREQUENCY.

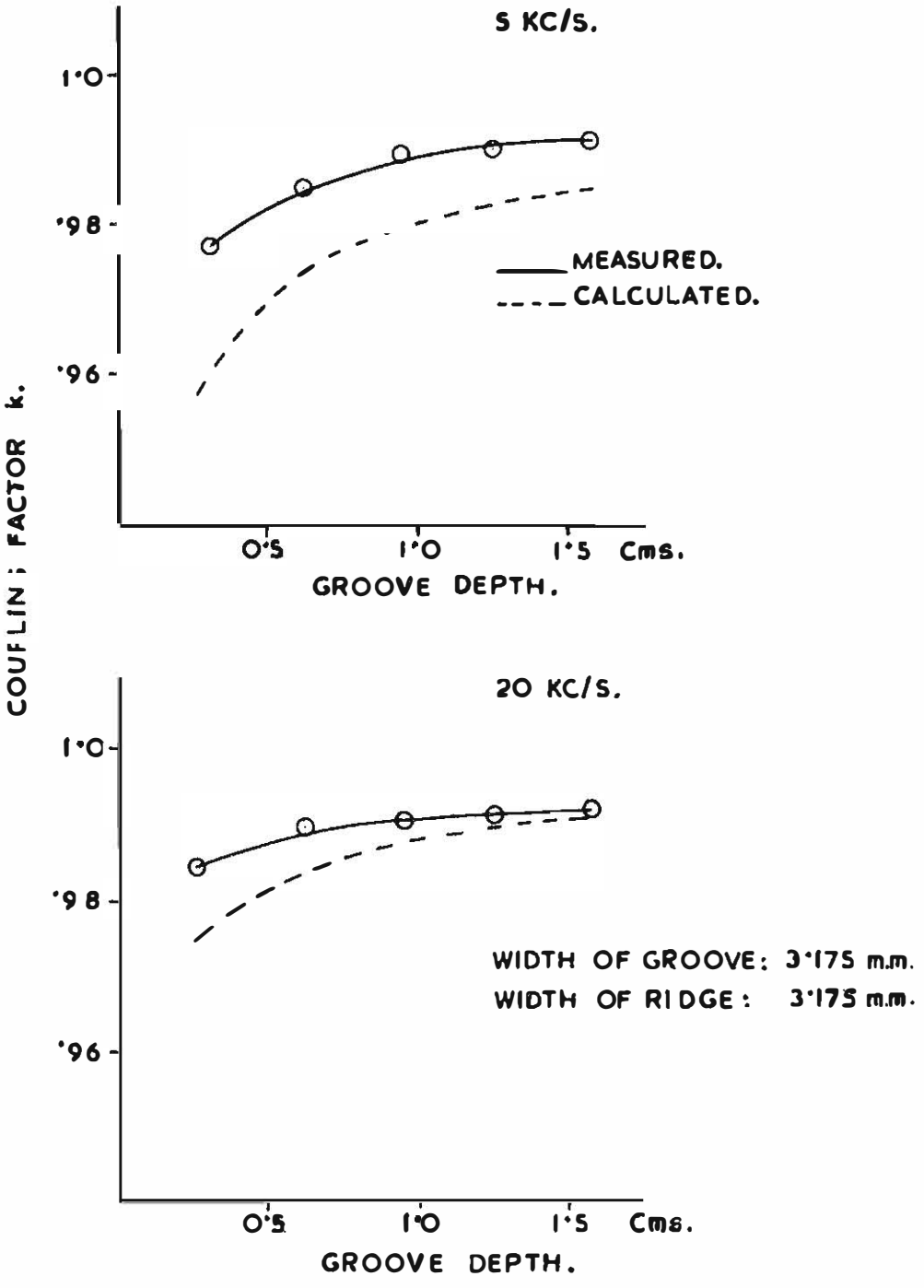

FIG. A3·6 VARIATION OF COUPLING WITH GROOVE DEPTH.

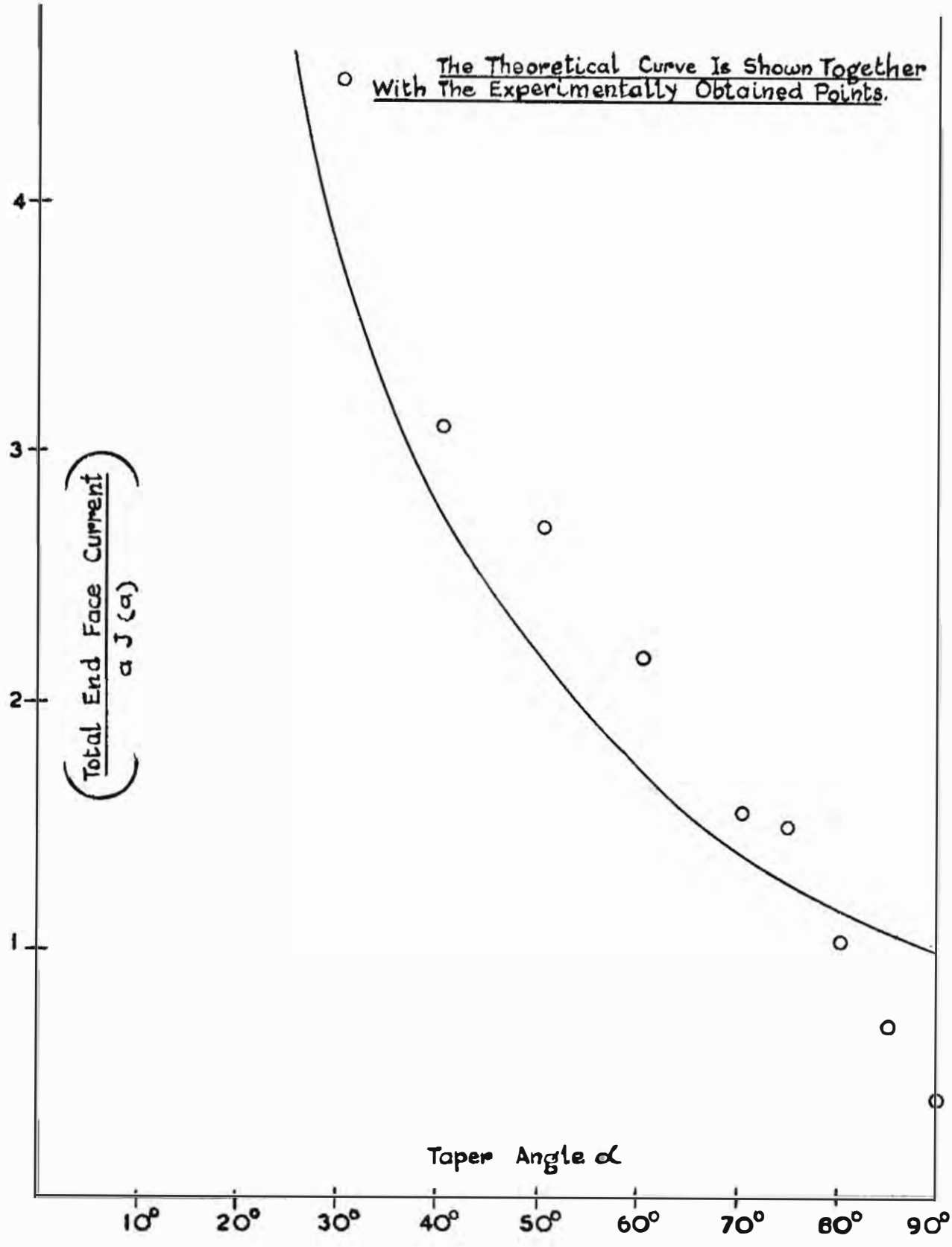

FIG. A3·7. END FACE CURRENT IN A TAPERED SLUG.